Silicon
https://doi.org/10.1007/s12633-022-02072-0

ORIGINAL PAPER

A Study of the Ceramicisation of Allylhydridopolycarbosilane by Thermal Volatilisation Analysis and Solid-State Nuclear Magnetic Resonance

Lewis J. Print[1] · John J. Liggat[1] · Stan Moug[2] · Helen Seaton[2] · David C. Apperley[3]

Received: 7 March 2022 / Accepted: 21 August 2022

Abstract
AHPCS is a pre-ceramic polymer utilised as a precursor to SiC. An initial polymerisation to a cross-linked network is followed by a complex sequence of processes ultimately leading to amorphous SiC. Using thermal volatilisation analysis (TVA) accompanied with solid-state NMR (SSNMR), FTIR, MS, DSC and TGA the complete thermal profile was identified. Between 160 – 300 °C, AHPCS cross-links through the allyl group and undergoes some carbon-silicon rearrangement, with a volatilisation of low mass oligomeric material and significant volumes of hydrogen released from dehydrocoupling of SiH moieties. By 300 °C the allyl group is completely cross-linked but the polymer starts to undergo pyrolytic degradation of the network, with the release of chain fragments and low molar mass species such as methane, ethane, methanol, propane, propene and silane species. Hydrogen once again becomes the major volatile product above 400 °C due to higher proportion of dehydrocoupling forming Si–C and Si–Si bonds. Small chain fragments are seen in the form of larger alkyl silanes. These fragments come from the chain scission of the polymer at weaker parts of the network. The process of side group scission leads to further radical recombination reactions of silicon and carbon atoms to build the SiC network. By 500 °C higher proportion of dehydrocoupling occurs with recombination of Si–Si and Si–C species. The Si–H bonds in -SiH_3 groups have completely cleaved along with C-H bonds in the CH_3 and CH_2 groups leaving SiC, -SiH and $HCSi_3$ present in the material. This bond cleavage leads the silicon and carbon radical species to undergo radical recombination in the network with the volatile release being dominated by H_2. By 650 °C the cleavage and recombination of remaining -SiH_2-, -SiH- and $HCSi_3$ groups ultimately form amorphous SiC. The volatiles released are mostly hydrogen with very few condensable products seen. Finally, SiC is then crystallised at higher temperatures forming β-SiC at 1100 °C and then subsequently α-SiC above 1500 °C.

Keywords Silicon carbide · Evolved gas analysis · Thermal analysis · Polycarbosilane

1 Introduction

Silicon-based ceramics have unique properties which make them extremely useful in many different applications and as such have attracted great interest [1–4]. Silicon carbide is an advanced structural ceramic that has very high hardness and strength as well as having a high resistance to corrosion [5].

Silicon carbide was first synthesized by Edward Acheson, in 1892, by mixing silica sand and petroleum coke in a furnace at around 2300 °C [6, 7]. This Acheson process has been used in the production of silicon carbide ever since. However, new methods of generating dense silicon carbide have since been developed using pre-ceramic polymers [8]. Pre-ceramic polymers have the advantage of generating useful and unconventional structures with ease at lower temperatures.

Polycarbosilanes are a unique class of polymers, with a backbone consisting of adjacent silicon and carbon atoms as seen in Fig. 1.

The R and R' side groups can vary from alkyl, aryl, alkoxy groups or hydrogen and halogen atoms. These side groups can be used as bridging points in the polymer to

✉ John J. Liggat
j.j.liggat@strath.ac.uk

[1] Department of Pure and Applied Chemistry, University of Strathclyde, Glasgow G1 1XL, Scotland, UK

[2] Sandvik Ltd T/A Kanthal, Inveralmond, Perth PH1 3ED, Scotland, UK

[3] Department of Chemistry, Durham University, Lower Mountjoy, Stockton Road, Durham DH1 3LE, UK

Published online: 17 September 2022

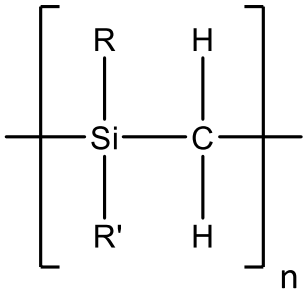

Fig. 1 Basic PCS repeating structure

form cross-links in the structure upon heating e.g. methylene bridges from vinyl/allyl groups. These different structures can produce polymers with interesting properties compared to normal hydrocarbon-based polymers. A significant application for polycarbosilanes is their use as a ceramic precursor for silicon carbide.

Much research has been conducted and reported in papers concerning polycarbosilanes, their thermal behaviour and ceramicisation process [9–12]. The ceramic yield from the precursors is influenced by the functional groups and cross-linking degree of the polymer. The ideal structure for the silicon carbide precursor is a pre-existing backbone of alternating silicon and carbon atoms with substituents appropriate for building a 3-D network. A liquid precursor that can be cured to an initial cross-linked network facilitates the shaping of complex parts. This network is then pyrolyzed to generate the silicon carbide [13]. Allylhydridopolycarbosilane (AHPCS) is a partially substituted pre-ceramic polymer with a composition of 10 mol% allyl present as a functional group. The simplified structure is shown in Fig. 2 although

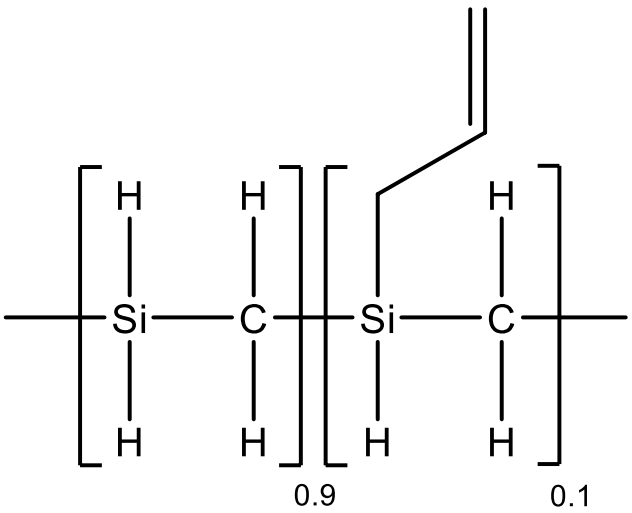

Fig. 2 Simplified structure of AHPCS

in the commercially available material used here some -Si(CH_3)H-units are also present along the backbone [14].

The formation of SiC from AHPCS typically occurs via two main processes, the initial cross-linking through the allyl group to generate the precursor network followed by the ceramicisation process. In the cross-linking step of AHPCS, two mechanisms are operable. The first is polymerisation of the allyl group via a free-radical mechanism to form the thermoset polycarbosilane material at approximately 140–250 °C, which is shown in Scheme 1 [14]. Alternatively, hydrosilation of the double bond and dehydrocoupling are determined by Kaur *et al.* as being the main mechanisms that contribute to the cross-linking reactions during heating to form the SiC, Scheme 2, [15, 16]. The first route is amenable to acceleration through the use of free-radical initiators [17].

In the ceramicisation process, the SiC is obtained through direct dehydrocoupling and recombination reactions of radical species generated by the pyrolysis of the precursor network, Scheme 3. This generates amorphous SiC, which then crystallises to form β-SiC at 1600 °C. Temperatures exceeding 1700 °C cause the SiC to rearrange to form α-SiC [11, 18]. This dehydrocoupling can also produce silicon-centre to silicon-centre recombination which is an unwanted side-reaction that can increase the Si content of the final ceramic [15].

Although the general process for the cross-linking and ceramicisation of polycarbosilanes is known, the specific reactions that occur at different temperature ranges are not fully understood as many of the studies focus on the higher temperature processes. Establishing the complete thermal profile of AHPCS can play a vital role in optimising other pre-ceramic polymers in their synthesis and design as well as the use of other additives such as boron or titanium. In this study, to better understand the condensed-phase chemistry, a combination of volatile and residue analysis was conducted over the temperature range RT to 690 °C. Over this temperature range, the volatile evolution relates to three specific processes, the first is the cross-linking reaction to form the precursor network, the second is the pyrolysis of this network with the generation of new Si–C bonds with the volatilisation of fragments from the hydrocarbon parts of the network and the release of hydrogen from dehydrocoupling reactions, and the final is the completion of the conversion to SiC, with the production of further hydrogen. Understanding these process is of critical importance in the fabrication of SiC devices. Volatile evolution can produce unwanted voids, Si–H to Si–H dehydrocoupling can generate localise Si inclusions at the expense of Si–C bond formation and of course the evolution of hydrogen is a safety hazard. By providing a continual and extended real-time characterisation of the volatile species, Thermal Volatilisation Analysis, a technique unique to our laboratories, provides an unprecedented and unique insight into these processes and the underlying condensed phase chemistry.

Scheme 1 Free-radical cross-linking reaction mechanism of AHPCS vinyl groups at temperatures above 140 °C with the dashed lines representing the rest of the polymer chains

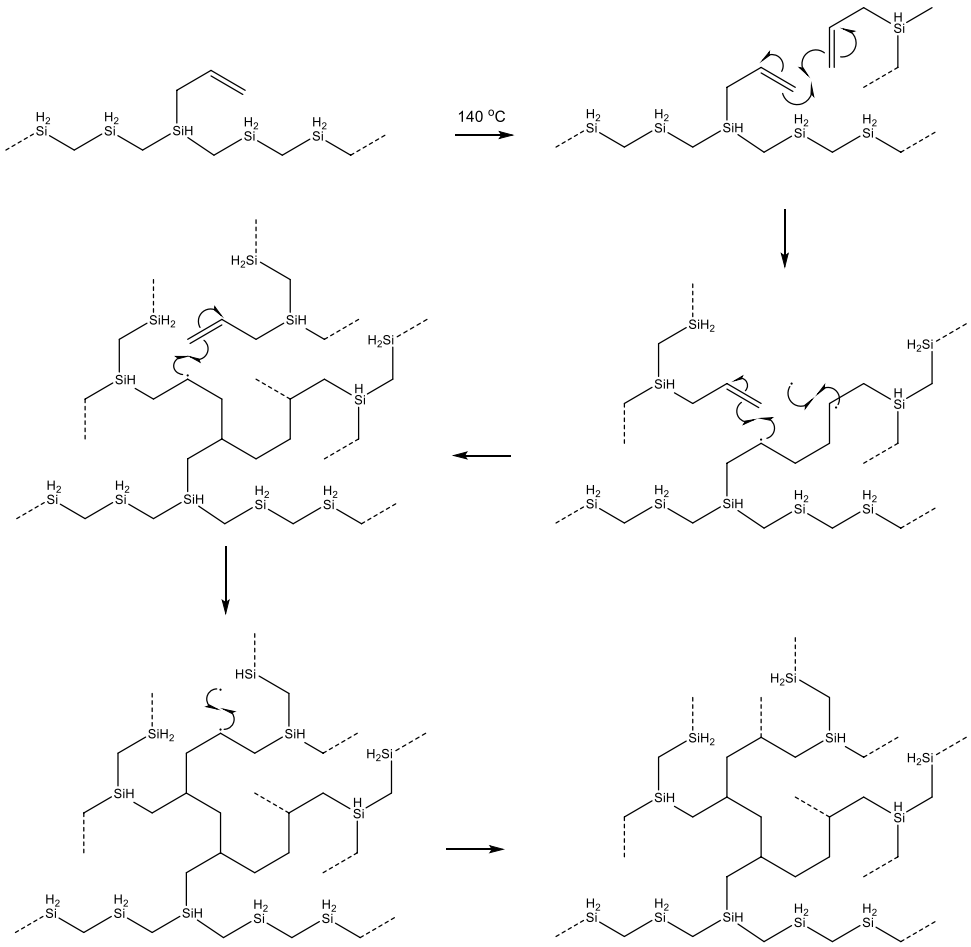

Scheme 2 Hydrosilation (**a**) and dehydrocoupling (**b**) routes to cross-linking of AHPCS

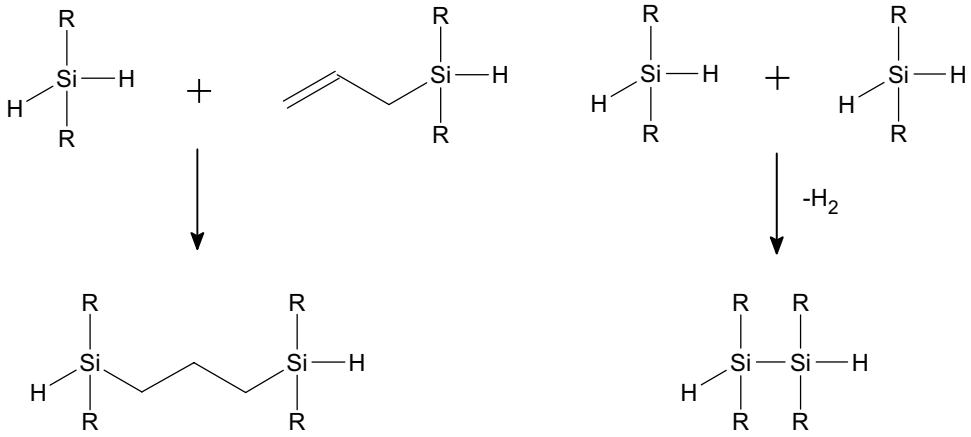

2 Experimental

2.1 Materials

The polycarbosilane used for this research was an allylhydridopolycarbosilane (SMP-10) supplied by Starfire Systems Inc. The material was characterised by gel permeation chromatography (GPC) prior to use.

2.2 Thermal Volatilisation Analysis (TVA)

All TVA analyses were carried out using a TVA line which was built in-house at the University of Strathclyde, based

Scheme 3 Silicon-hydrogen bond cleavage and subsequent radical recombination of silicon and carbon atoms in AHPCS

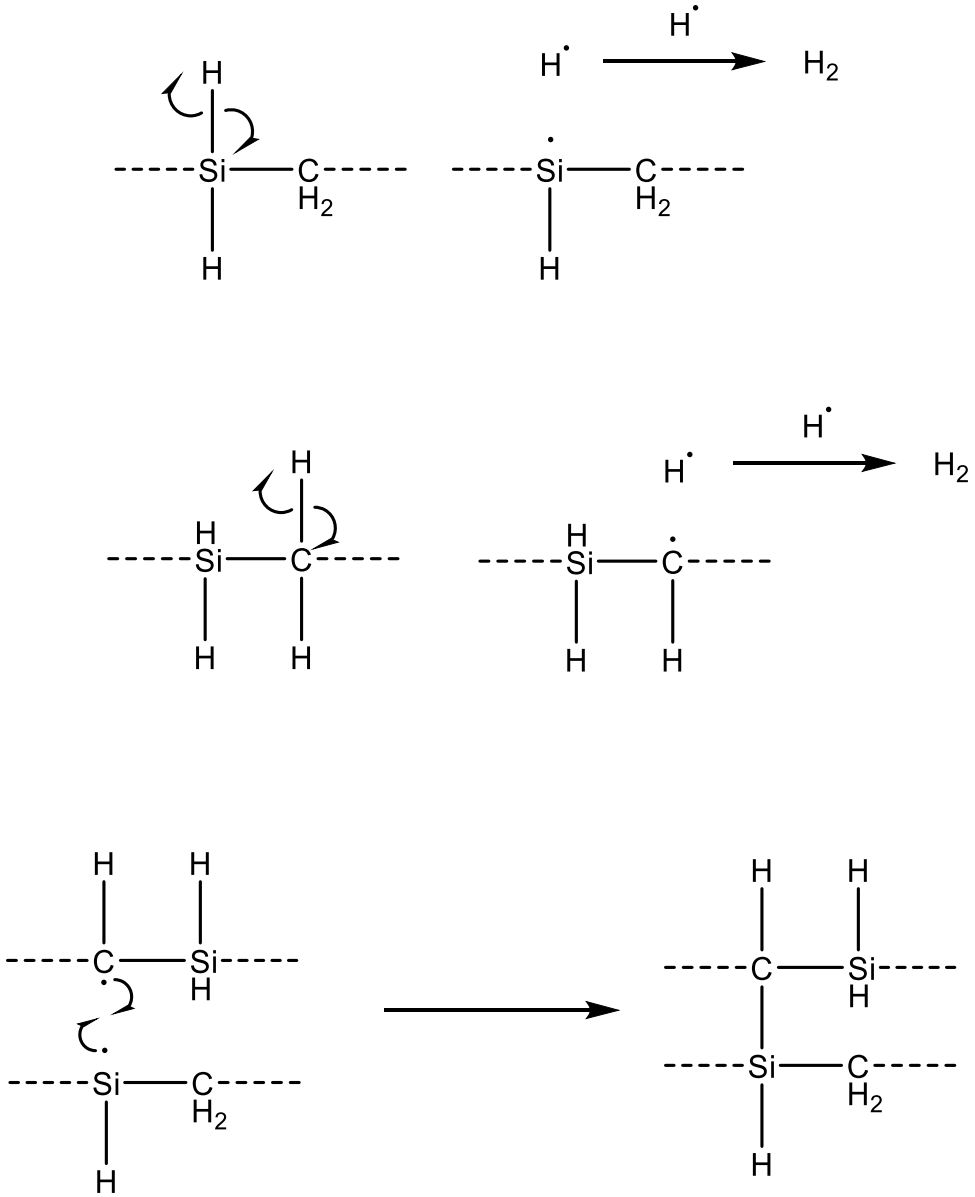

upon the apparatus and techniques described by McNeill et al. [19].

The apparatus, which is shown in Fig. 3, consists of a sample chamber, heated by a programmable tube furnace, connected in series to a nitrogen cooled sub-ambient trap. This primary sub-ambient trap can then be separated into four parallel, secondary liquid nitrogen cooled sub-ambient traps. The whole system is continuously pumped to a vacuum of approximately 1×10^{-4} mbar by a two-stage rotary pump and oil diffusion pump.

There are two stages in which volatile condensable products can be trapped and collected: a water jacket cooled by a chiller at the top of the heated sample tube, referred to as the cold-ring fraction, and the primary liquid nitrogen cooled sub-ambient trap. The higher boiling point volatile products that condense under vacuum at ambient temperature (~ 5 °C) are collected in the cold-ring fraction. The lower boiling point volatile products which do not condense under vacuum at ambient temperature but which condense under vacuum at liquid nitrogen temperatures (-196 °C) are collected in the sub-ambient trap.

Linear-response Pirani pressure gauges are positioned before and after the primary sub-ambient trap to measure the volatile evolution, which is recorded as the change in pressure as a function of temperature/time. The Pirani gauge before the sub-ambient trap measures the evolution of total volatiles from the sample and the Pirani gauge after the sub-ambient trap measures the evolution of non-condensable volatiles from the sample. Pressures are typically plotted as a function of temperature (time for

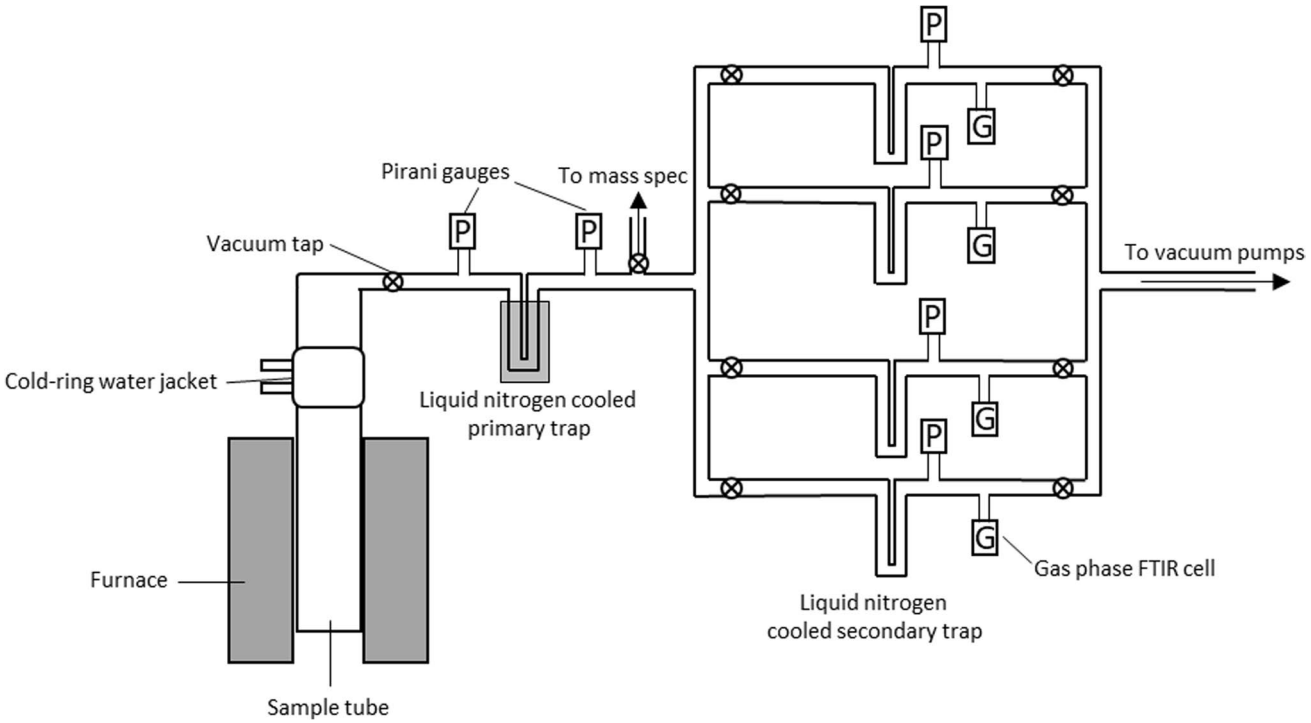

Fig. 3 Schematic diagram of the full TVA-SAD line used for the experiments

isothermal experiments) and integration of peak areas can be used to quantify the volatiles.

The sub-ambient trapped volatiles can be separated into the four limbs by slowly heating the primary liquid nitrogen trap to ambient temperature. These separated volatiles can be analysed subsequently by mass spectrometry and trapped in gas-phase cells for FTIR analysis. The volatiles, for each separate limb, are monitored by non-linear Pirani gauges as they distil into the gas-phase cells.

All TVA analyses were conducted under vacuum using 500 mg sample sizes. The heating ramp rate for the dynamic TVA run was 10 °C min^{-1} from ambient to 690 °C. Isothermal TVA experiments were carried out by heating to various temperatures, at a heating ramp rate of 10 °C min^{-1} and held iso-thermally for approximately 1–2 h. The step-wise isothermal TVA experiments were performed on the same sample, allowing the sample to cool and then reheating to the next isothermal temperature. The temperatures used for the isothermal experiments were 160, 300, 500, and 650 °C. A 1–300 Da, Hiden Analytical, single quadrupole RGA mass spectrometer was used to constantly analyse the volatiles for both the non-condensable TVA run and sub-ambient distillation cold trap. The dynamic TVA run was also repeated with the mass spectrometer used in MID mode to measure the different fragment concentrations as a function of temperature. The sub-ambient distillation products were collected into gas cells with sodium chloride windows and analysed using a PerkinElmer Spectrum 100 FTIR spectrometer in transmission mode with an average of 16 scans and a resolution of 4 cm^{-1}.

2.3 Thermogravimetric Analysis-Differential Scanning Calorimetry (TGA–DSC)

All TGA–DSC analysis was carried out using a Netzsch, STA 449 F1 Jupiter thermal analyser using approximately 5 mg sample sizes. The samples were placed in platinum crucibles and heated using a ramp rate of 10 °C min^{-1} from 30 to 1500 °C under a flow of 50 ml min^{-1} argon. The mass loss was recorded as a function of temperature. From the TGA curve the first derivative was obtained and plotted as a function of temperature. Onset temperatures of reactions were determined using the derivative plot.

2.4 Attenuated Total Reflection Fourier-Transform Infrared (ATR-FTIR) Analysis

ATR-FTIR spectra were collected using an Agilent 4500A series ATR-FTIR instrument equipped with a reflective diamond (single bounce) ATR crystal. An average of 64 scans was used for collecting the background and sample spectra with a resolution of 4 cm^{-1} and a spectral range of 650 – 4000 cm^{-1}. Small samples were placed on the crystal and clamped down. The spectra were then normalised and baseline corrected using KnowItAll.

2.5 Gel Permeation Chromatography (GPC)

GPC analysis was conducted at the Pure and Applied Chemistry Department in the University of Strathclyde, using a PSS SECurity^2 GPC system, equipped with a refractive index detector, in a PSS GRAM analytical linear column, with dimensions of 8 × 300 mm with a 10 µm particle size, thermostatted to 35 °C. The mobile phase used was DMF with 50 mM lithium bromide with a flow rate of 1 ml min^{-1}. The samples were prepared in THF as the solvent at a concentration of 2 mg ml^{-1}.

2.6 Solid-State Nuclear Magnetic Resonance (SSNMR)

Solid state NMR experiments were performed at the ESPRC National Solid-State NMR service at Durham University. ^{13}C and ^{29}Si magic-angle spinning (MAS) and cross polarisation (CP-MAS) measurements were carried out on a Varian VNMRS spectrometer with a 6 mm (rotor o.d.) MAS probe operating at 100.55 and 79.44 MHz respectively. This probe enabled a spin rate of 6 kHz for all samples. The contact time for CP-MAS measurements was 1 and 5 ms for ^{13}C and ^{29}Si respectively. The recycle delay was 1.5 s for all samples. Spectral referencing is relative to neat tetramethylsilane, carried out by setting the high-frequency resonance from adamantane to 38.5 ppm (carbon) or the high-frequency resonance from tetrakis(trimethylsilylsilane) to -9.9 ppm (silicon).

2.7 X-ray Diffraction (XRD) Analysis

XRD patterns were collected using a Bruker D8 Advance X-ray Diffractometer, with Cu K_α incident radiation ($\lambda = 1.54$ Å). A tube accelerating voltage of 40 kV and 35 mA was used. The XRD patterns were recorded with a 2θ range of 20—95° and a step size of 0.05° every 5 s.

The XRD samples were prepared by pyrolysing the AHPCS at 1100, 1300, 1500 and 1700 °C under vacuum for half an hour. The samples were then ground up using a mortar and pestle to make a powder suitable for analysis. The XRD spectra were baseline corrected using DIFFRAC. SUITE software.

2.8 Sample Preparation of AHPCS for TVA analysis

Samples were prepared by holding 500 mg of the material under a vacuum for two days to ensure maximum volatilisation of the lower molecular mass oligomer material that is present in commercial AHPCS (see Sect. 3.1). This was done to achieve the high vacuum needed for the TVA and reduced the complication of unreacted oligomer volatilising alongside the reaction products.

3 Results and Discussion

3.1 GPC of AHPCS

The molecular mass and polydispersity of AHPCS were measured using GPC to create a profile of the starting material shown in Fig. 4. The as-received material contains a significant low molecular mass component. Holding the sample at room temperature under vacuum in the TVA at 1×10^{-2} mbar for two days helps distils off this component as can be seen in Fig. 4. This made sure that any volatiles produced during heating were due to the reactions and not that of unreacted oligomers. The unreacted oligomers that condensed at the cold-ring trap were collected and analysed with the comparison to the higher molecular mass polymer that was kept under vacuum and the as received AHPCS. The data analysis is tabulated in Table 1.

As expected, the distillate from the vacuum treatment has a lower number average molecular mass than the residual material, the vacuum treatment having removed the low molar mass tail. The origin of the high molecular mass peaks seen about 100,000 Da is unclear but may indicate that some cross-linking chemistry occurs upon storage at room temperature.

3.2 TGA of AHPCS

TGA was used to study the overall thermal profile of AHPCS under non-oxidative conditions and to observe the mass loss steps from the polymer. These mass loss processes are believed to be related to the formation of the cross-linked polymer from the oligomers and the subsequent formation of amorphous SiC [20]. In Fig. 5, the TGA mass loss curve is shown of the AHPCS (as received) with the corresponding first derivative curve (DTG). The mass losses occur in four distinct steps. The first mass loss step occurs at 50 – 300 °C and is attributed to a combination of the loss of low molecular mass oligomer species in the mixture and production of volatiles upon the initiation of cross-linking. The second mass loss step which occurs at 300 – 600 °C has been attributed to the cleavage of side groups, with the release of volatile products such as methane and silane species as well as the start of dehydrocoupling which releases hydrogen. The third mass loss step occurring at 600 – 900 °C is believed to be from the complete dehydrocoupling of the C-H and Si–H bonds [14]. From 1000 – 1200 °C the fourth mass loss step is understood to occur as a result of the loss of the oxycarbide phase in the SiC structure, releasing SiO_2 and CO [21]. The oxycarbide phase comes from the synthesis and processing of AHPCS in which as much as 7% oxygen can be incorporated into the polymer [15]. The overall ceramic yield obtained from the AHPCS is 70% at 1500 °C.

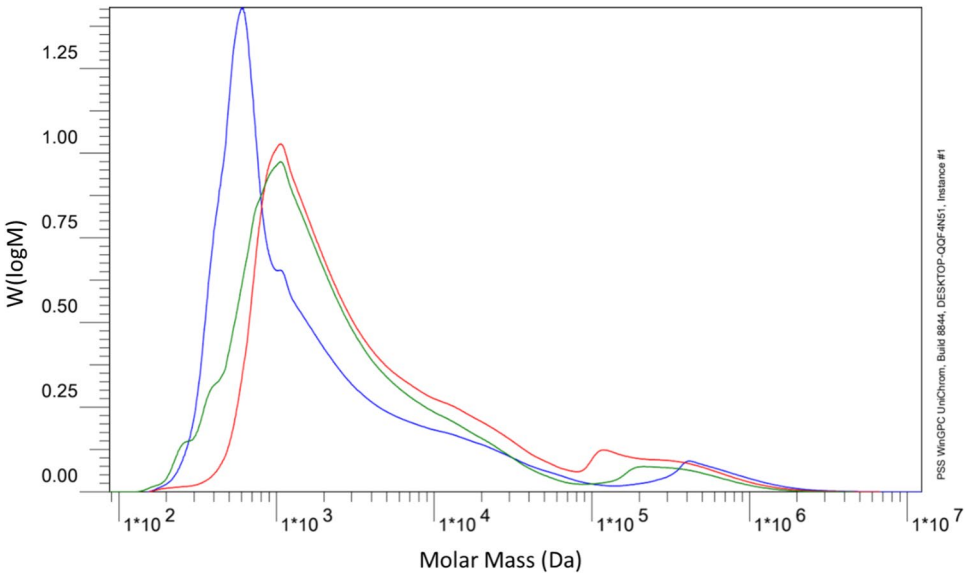

Fig. 4 GPC chromatogram of AHPCS as received (green), AHPCS under vacuum for two days (red) and the AHPCS distillate collected after two days (blue)

Table 1 GPC analysis of AHPCS

AHPCS analysed	Number average molecular mass (g mol^{-1})	Weight average molecular mass (g mol^{-1})	Polydispersity
AHPCS	1195	27,449	2.3
AHPCS under vacuum	1770	42,032	2.4
AHPCS distillate	905	41,463	4.6

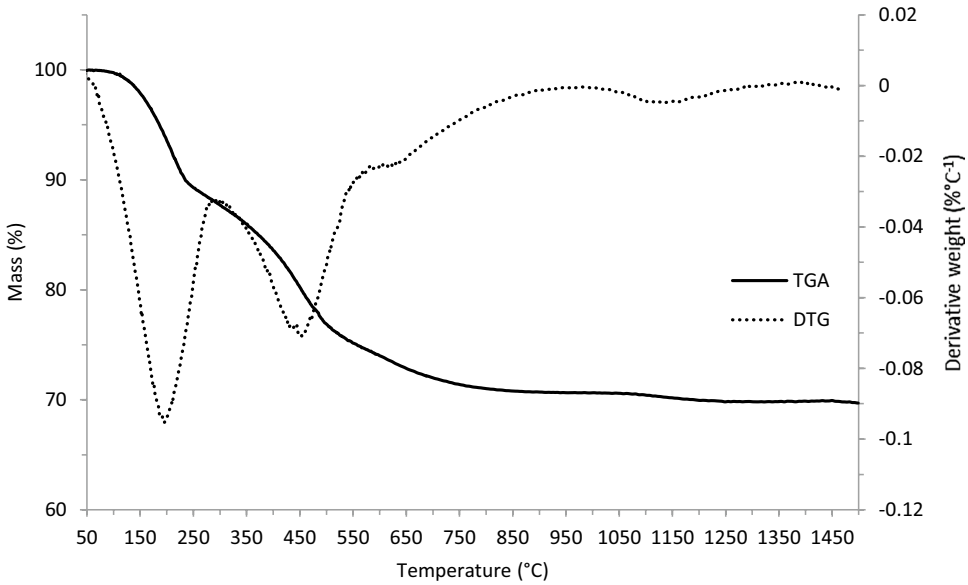

Fig. 5 TGA/DTG of AHPCS in argon gas up to 1500 °C

3.3 DSC of AHPCS

The DSC in Fig. 6 shows the thermal profile of AHPCS (as received). From 25 to 100 °C there is a slight endothermic process that is attributed to the volatilisation of low molecular mass oligomer species. The first exothermic peak, at 240 °C, is attributed to the cross-linking of the vinyl groups on the polymer chain. The endothermic and exothermic peaks that occur between 400 and 700 °C can be accounted for by the release of the gaseous products and the recombination of silicon and carbon radical species respectively. At 1072 °C, the exotherm is most likely caused by structural

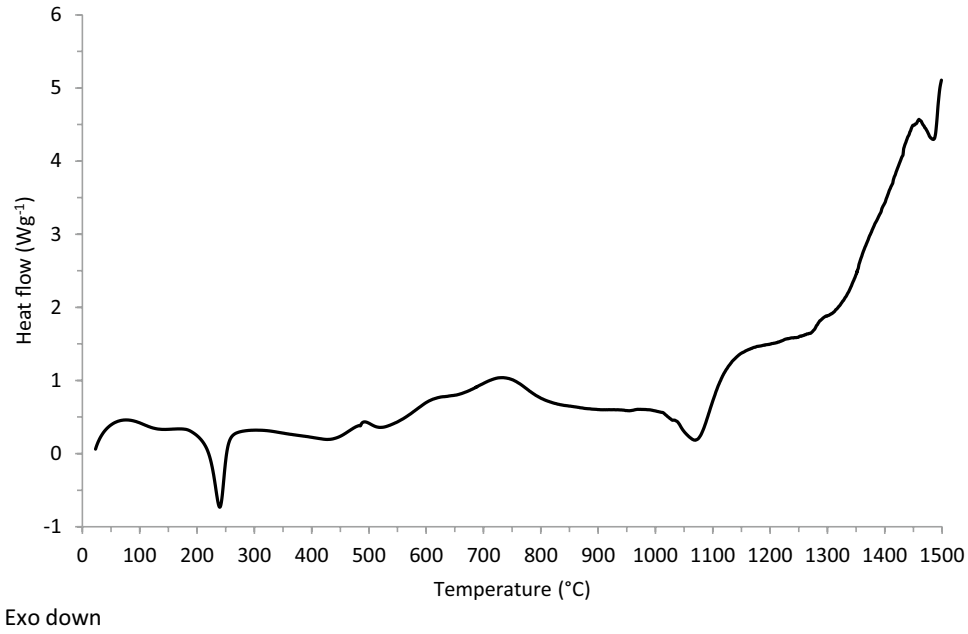

Fig. 6 DSC of AHPCS in argon gas up to 1500 °C

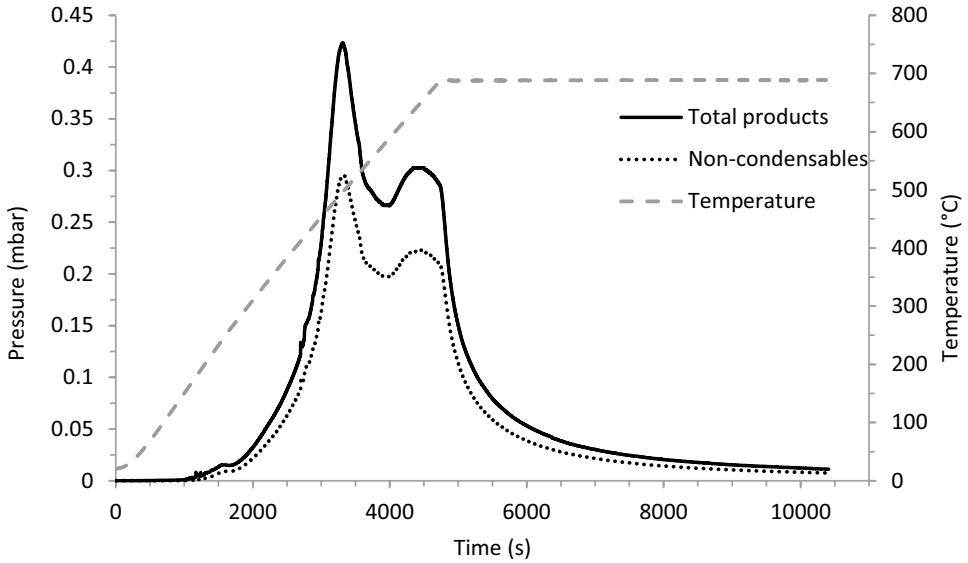

Fig. 7 Dynamic TVA curve up to 690 °C

relaxation and condensation of the amorphous SiC prior to crystallisation [22, 23]. The SiC is still amorphous at this temperature, as outlined by Nguyen et al. during a thermal analysis study of AHPCS using XRD [24, 25]. The broad endotherm from 1270 – 1460 °C is a result of the loss of the oxycarbide phase (Si–O-C), consistent with the TGA data in Fig. 5. The exotherm at 1485 °C is due to the complete crystallisation of the amorphous SiC to form the β-SiC [26].

3.4 TVA of AHPCS

Using TVA, the thermal behaviour of materials can be monitored under vacuum. This allows full characterisation of reactions that occur upon heating. Volatile degradation products are recorded as they evolve. The condensable and non-condensable products were measured using MS during the TVA run.

Table 2 Key TVA temperature events for AHPCS

TVA curve event	Onset temperature (°C)	Peak maximum (°C)
Event 1	~150	~300
Event 2	~250	~500
Event 3	~595	~650

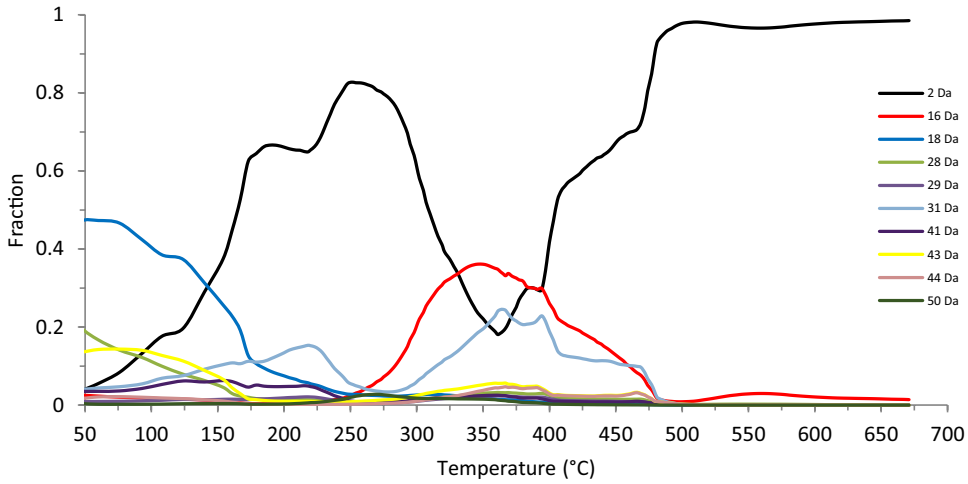

Fig. 8 MS fraction of major fragments evolved during the full dynamic TVA run

In Fig. 7, the dynamic TVA curve is shown from room temperature to 690 °C. It shows the evolution of volatiles produced from reactions as a function of temperature. There are four main temperature events, three of which are seen in the TVA curve, and highlighted in Table 2. These four events represent the three different reactions occurring – the initial and complete cross-linking, initial ceramicisation process and the complete ceramicisation which also correspond to peaks seen in the DSC and DTG. The initial cross-linking to form the precursor network occurs between 140–160 °C, which produces a slightly flexible partially cross-linked polymer. This first thermal event can be noted by the release of non-condensables immediately suggesting that the dehydrocoupling reaction is involved in this initial cross-linking step. The first small peak is seen as a shoulder around 250–300 °C to the second and largest peak at around 500 °C. The third peak sits at around 650 °C. The apparent drastic increase in pressure is from the ceramicisation dehydrocoupling reactions which release hydrogen as a non-condensable. This is because the thermal conductivity of H_2 is much higher than most other gases (0.1866 W m^{-1} k^{-1} compared to nitrogen at 0.026 W m^{-1} k^{-1} at room temperature). This affects the Pirani output readings which are uncorrected for the gas type, exaggerating the quantity of hydrogen relative to other gases [27].

From the full MS run the major products released are shown in Fig. 8. Volatile production is dominated by the hydrogen evolution (2 Da) but also includes other small molecules such as methane (16 Da) and propane fragments (29 Da) with small amounts of other fragments (MeCl – 50 Da, MeSi – 44 Da, CH_3O – 43 Da, propene – 41 Da, methanol/SiH_4 – 31 Da, ethane – 28 Da). The

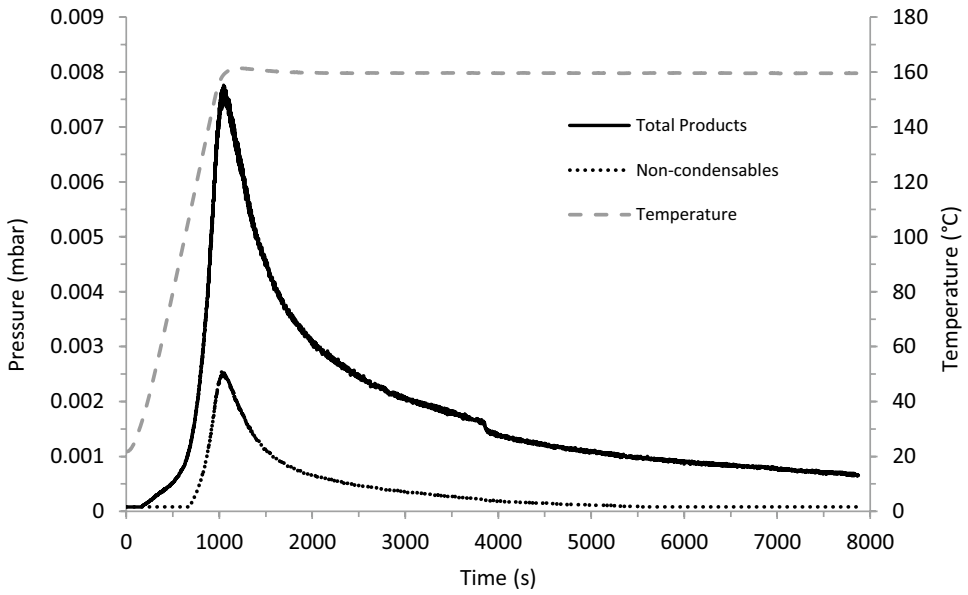

Fig. 9 Isothermal TVA curve for AHPCS heated at 160 °C

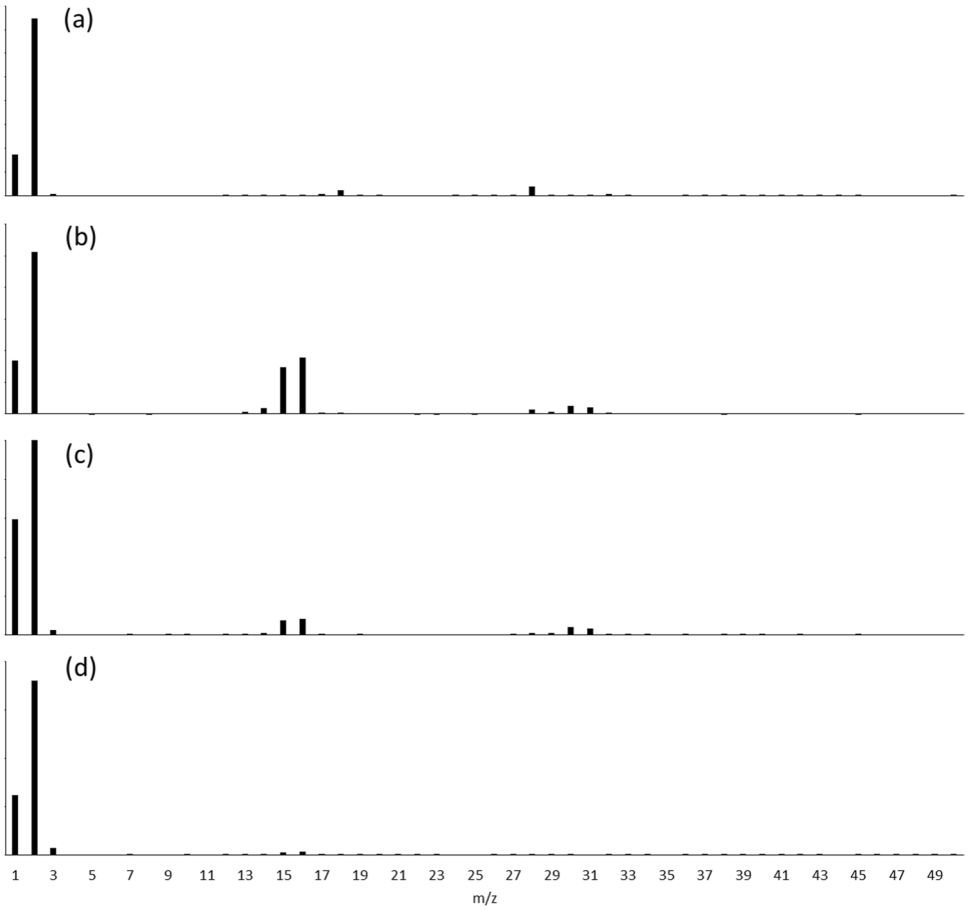

Fig. 10 MS of non-condensable products from 160 °C (**a**), 300 °C (**b**), 500 °C (**c**), 650 °C (**d**) TVA isothermals

water (18 Da) stems from a combination of residual water in the sample and water degassing from the glass walls of the TVA line as it heats. It is hard to identify the exact compounds from the MS due to the similar fragmentation patterns observed.

3.4.1 Isothermal Thermal Volatilisation Analysis

To better understand the detailed chemistry occurring, stepwise isothermal runs were performed at the key temperatures in order to analyse the volatile products and examine the

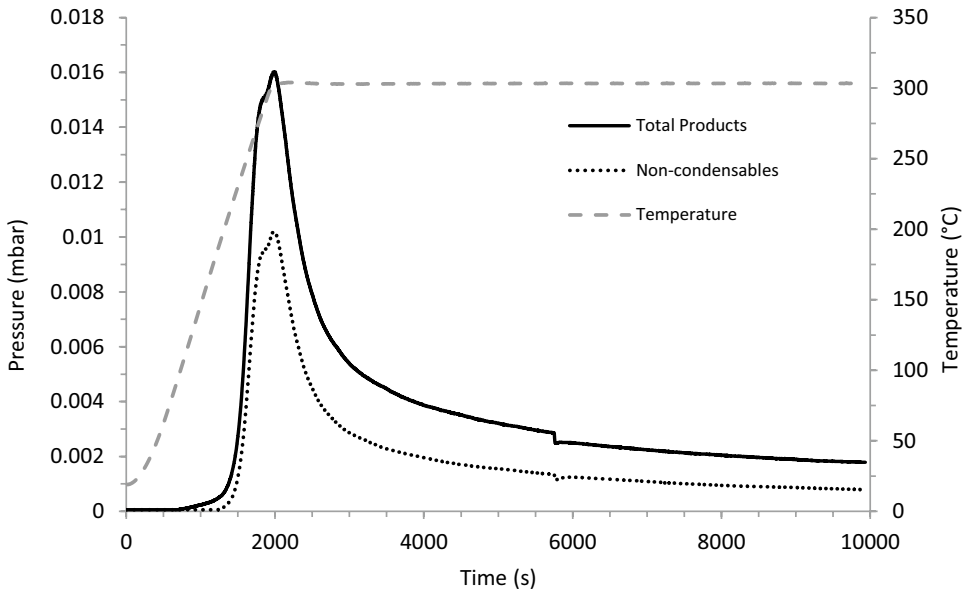

Fig. 11 Isothermal TVA curve for AHPCS heated at 300 °C

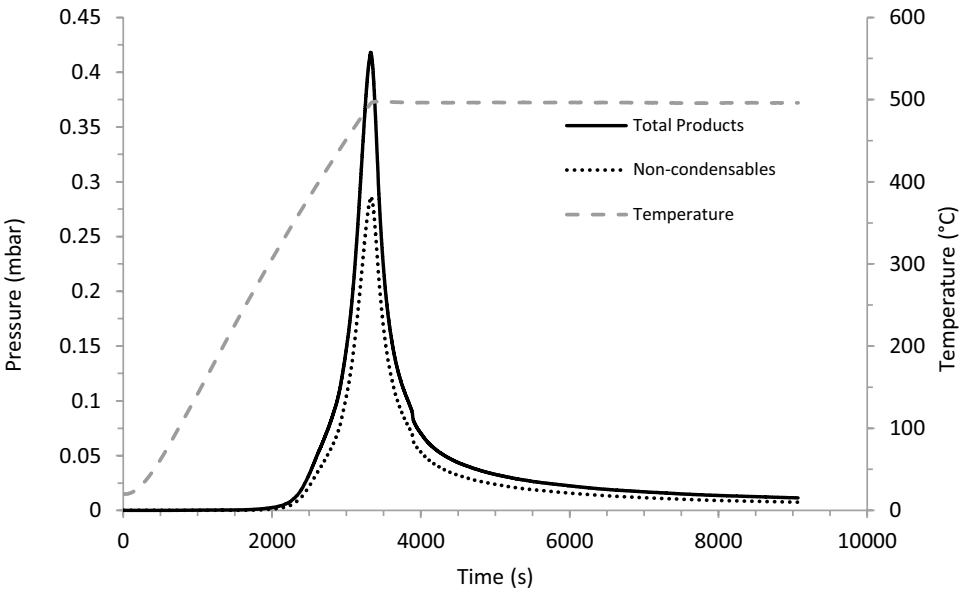

Fig. 12 Isothermal TVA curve for AHPCS heated at 500 °C

reactions undergone in the polymer. The mass spectrometry data for the non-condensable products were also recorded.

The isothermal temperatures used for the study corresponded to the peak maxima from the dynamic TVA run (160, 300, 500 and 650 °C). FTIR spectroscopy and MS were used to identify the products. The 160 °C curve from Fig. 9 corresponds to the initial cross-linking of the allyl groups on the polymer chain. The non-condensable products recorded are due to the loss of hydrogen from -SiH_2/SiH_3 moieties, resulting in Si–C cross-links as has been outlined previously by R. Sreeja et al.[14]. The volume of volatiles is low at 160 °C in comparison to the other temperatures (maximum pressure is 0.008 mbar) and H_2 accounts for a small part of that recorded in the MS as seen in Fig. 10. At 300 °C the allyl groups are predicted to completely react and cross-link to form a thermoset 3-D structure, releasing more non-condensable products from the cleavage of small side groups, this TVA trace is shown in Fig. 11. The non-condensable groups recorded in the MS are a mixture of (mostly) H_2 and CH_4 The peaks at 30 and 31 Da are consistent with SiH_4, also reported over this temperature range by Kaur et al.[15]. The tailing seen in the TVA curves are a consequence of the time taken for the ongoing reactions to complete at the isothermal temperatures. The AHPCS polymer starts to degrade above 300 °C with the cleavage and volatilisation of side groups

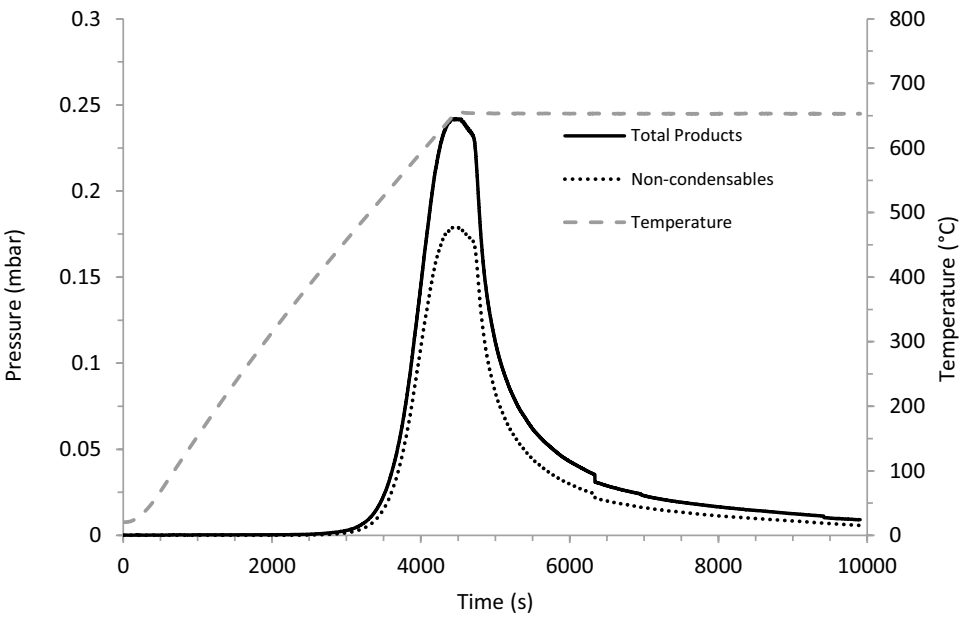

Fig. 13 Isothermal TVA curve for AHPCS heated at 650 °C

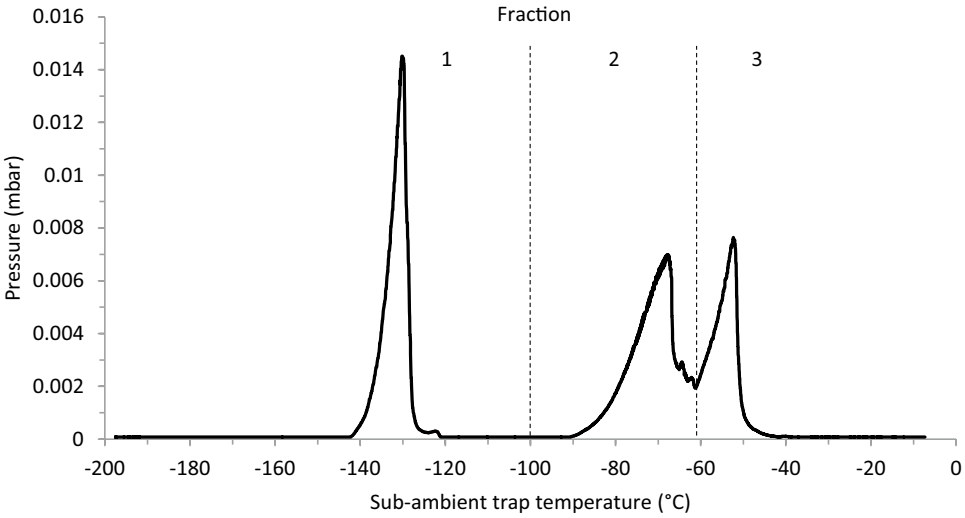

Fig. 14 SAD curve for the volatile products from the 160 °C isothermal TVA

which cause recombination reactions of silicon and carbon radicals to form a SiC network [11]. The major non-condensable product from 200 °C to 500 °C changes initially from H_2 to CH_4 which has a maximum at 350 °C, seen in Fig. 8. Hydrogen then begins to dominate again at temperatures above 400 °C, with a small trace of CH_4 visible for both the 500 °C and 650 °C isothermals and SiH_4 at 300 and 500 °C (Fig. 10). The reason for this change in non-condensable products is because at the lower temperatures below 300 °C, the hydrogen is accounted for by dehydrocoupling reactions, whereas the higher temperatures result in the cleavage of the stronger C–C bonds producing CH_4 and C_2H_6, from side group cleavage, and hydrogen, from the C-H bonds. Higher molecular mass species are given off, which are discussed further in Sect. 3.4.2.

Temperatures upwards of 300 °C (Figs. 12 and 13) seem to produce volatiles in much larger quantities. However, care must be taken in interpreting the TVA curves. As noted earlier, this is because the thermal conductivity of H_2 is 5 – 10 times higher than most other gases affecting the Pirani output readings which are uncorrected for the gas type [27].

3.4.2 Isothermal Sub-Ambient Distillation

The condensable volatile products from the isothermal runs were separated into fractions by sub-ambient distillation and analysed by FTIR and MS (Figs. 14, 15, 16, 17, 18, 19, 20, 21, 22, 23, 24, 25, 26).

In the SAD curves each peak represents a distinct component of the total volatile products collected. This trace is shown with

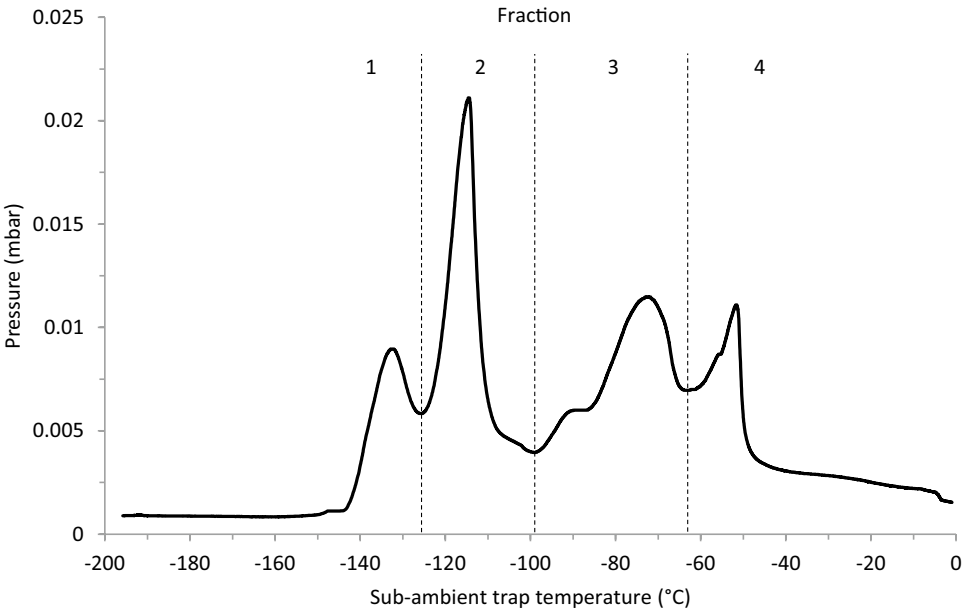

Fig. 15 SAD curve for the volatile products from the 300 °C isothermal TVA

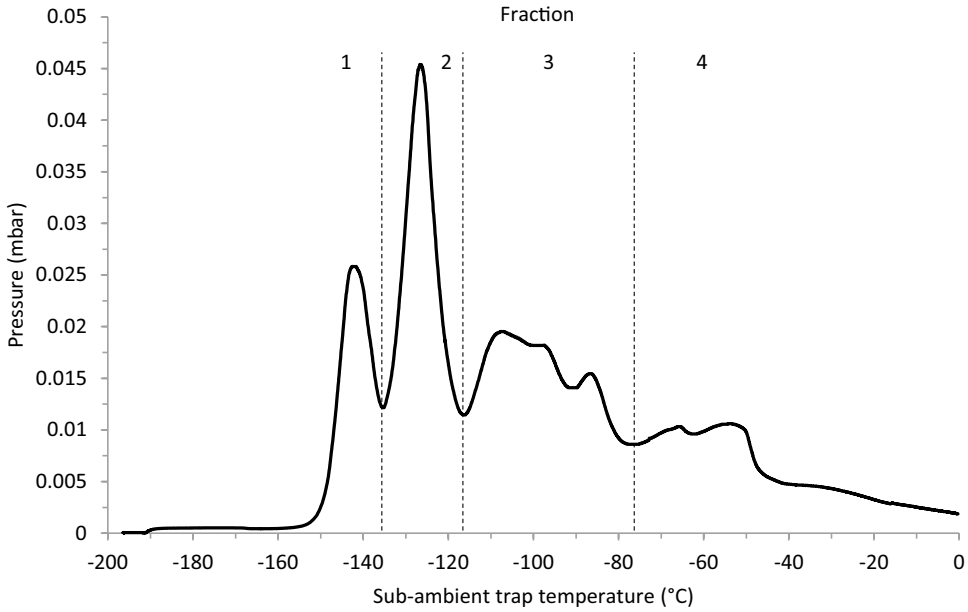

Fig. 16 SAD curve for the volatile products from the 500 °C isothermal TVA

the separate fractions in Figs. 14, 15, 16 and 17. The products were identified and characterised and are tabulated in Table 3.

At the first stage of the initial cross-linking of the polymer at 160 °C, the major volatiles produced are propene, methanol and water. The SAD curve is shown in Fig. 14 with the gas phase FTIR and MS shown in Figs. 18 and 22. A small volume of other volatiles (e.g. the THF) is evident and these are thought to be leftover impurities from the formation of AHPCS. The methanol may be either from unreacted methoxy groups that have not been reduced or from the side-product reaction that occurs during the synthesis with THF shown in Scheme 4 [28, 29]. The propene could be present due to unreacted side groups which may be cleaved from the allyl groups on the silicon backbone. Residual water may remain in the mixture from the washing step at the end of the synthesis.

After full cross-linking of the polymer network at 300 °C the polymer starts to undergo a series of chain scission and bond cleavage reactions, releasing small side groups and chain end groups. Propene is again recorded at this temperature and as before it is due to the loss of the allyl side groups from the main polymer chain which have not cross-linked to form the thermoset network. Chloromethane is detected which is a result of the leftover reactants from the Grignard coupling reactions in the synthesis of the polymer. Methyl- and ethyl-silane groups are present from the chain scission of the polymer due to the higher temperatures. Methanol is clearly observed in the FTIR (Fig. 19) and MS (Fig. 23),

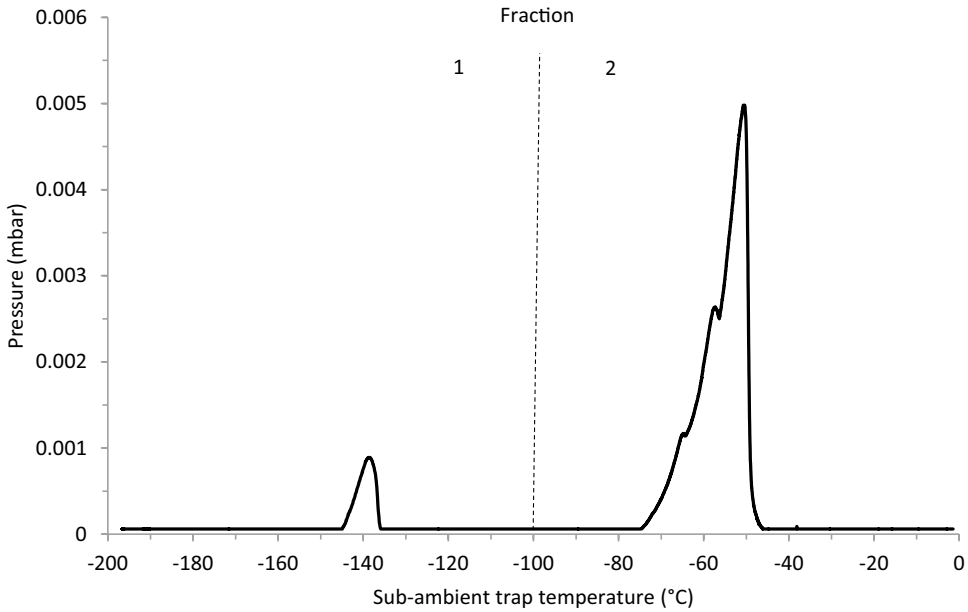

Fig. 17 SAD curve for the volatile products from the 650 °C isothermal TVA

Table 3 Condensable products identified from isothermal TVA experiments

Isothermal temperature (°C)	SAD temperature range (°C)	Products
160	(a) -196 to -100	Propene
	(b) -100 to -60	Methanol
	(c) -60 to 0	Water, large aliphatics
300	(a) -196 to -125	Methylsilane, Propene
	(b) -125 to -100	Chloromethane
	(c) -100 to -60	Methanol
	(d) -60 to 0	THF
500	(a) -196 to -135	Methylsilane
	(b) -135 to -115	Propene, ether silanes
	(c) -115 to -75	Propylsilane, ether silanes
	(d) -80 to 0	Large carbosilane fragments
650	(a) -196 to -100	Propane, Propene
	(b) -100 to 0	Large carbosilane fragments

highlighting that the polymer has larger chain fragments which have oxygen containing species in them: most likely silyl/alkyl ether groups from the use of THF in the synthesis reaction.

The largest volatile loss is seen from the 500 °C isothermal shown in Fig. 12. This is where the polymer begins to undergo major cleavage of bonds which then go on to form cross-links between the silicon and carbon atoms. The highest degree of bond cleavage and chain scission occurs at this higher temperature. The cross-linked network remains at 500 °C, however with very few aliphatic groups remaining. Both propene and propane are evident in the MS (Fig. 24) with propene being present in very small amounts. This shows evidence of the breakdown of the bridging chains between propyl groups and silicon atoms formed during the polymerisation step. Many silicon-based polymer derivatives are seen at this isothermal temperature such as methyl and ethyl silane. Chain scission of larger fragments are evident in the form of propyl silane, resulting from the degradation of fragments with the bridging propyl group, as well as silane, trimethylsilane, dimethylsilane, disilyl methane and methyl(silylmethyl) silane (Schemes 5 & 6). These larger fragments dominate the MS and FTIR data and are typical repeating units on the polymer backbone which have been cleaved from the main chain during the ceramicisation process. Small amounts of ether alkyl silanes are present, with the peak at 75 Da corresponding to C_2H_7OSi. At this point the cleavage results in the recombination of silicon and carbon atoms. From the MS data larger fragments are likely, with higher numbers of repeating units of the polymer chain above 100 Da. The SAD peaks (Fig. 16) are not as clearly defined at this temperature (or at 300 °C) due to the inability of the technique to fully separate products of similar volatility such as the range of fragments produced at 500 °C. The extended tail at higher temperature is due to the higher molecular mass fractions volatilising slowly over a long period of time.

At the final isothermal temperature, 650 °C, the SAD shows two main peaks in Fig. 17. At this temperature the final re-arrangement of the polymer occurs and the resulting material is an amorphous SiC network. Temperatures above 650 °C contribute to the crystallisation of SiC to produce β-SiC. Due to the low volume of volatiles in the SAD curve, the FTIR spectra in Fig. 21 show very little. The first peak seen in the SAD curve corresponds to CO_2 with a small amount of propane and propene which is observed in the MS

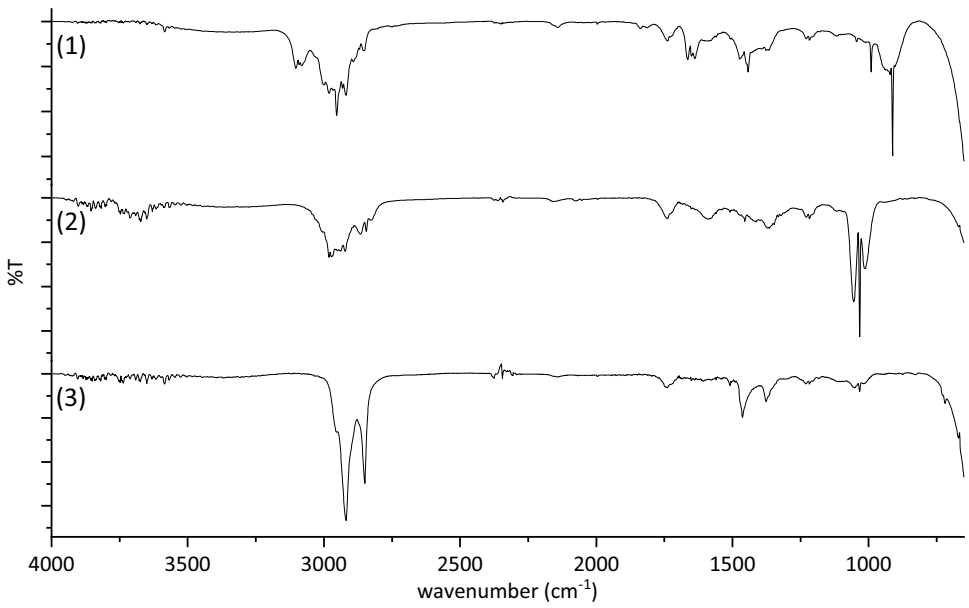

Fig. 18 FTIR gas phase spectra of the volatile SAD products in fractions 1, 2 and 3 from the 160 °C isothermal TVA

Scheme 4 Silylether side-product formation from the synthesis of AHPCS with THF as a solvent

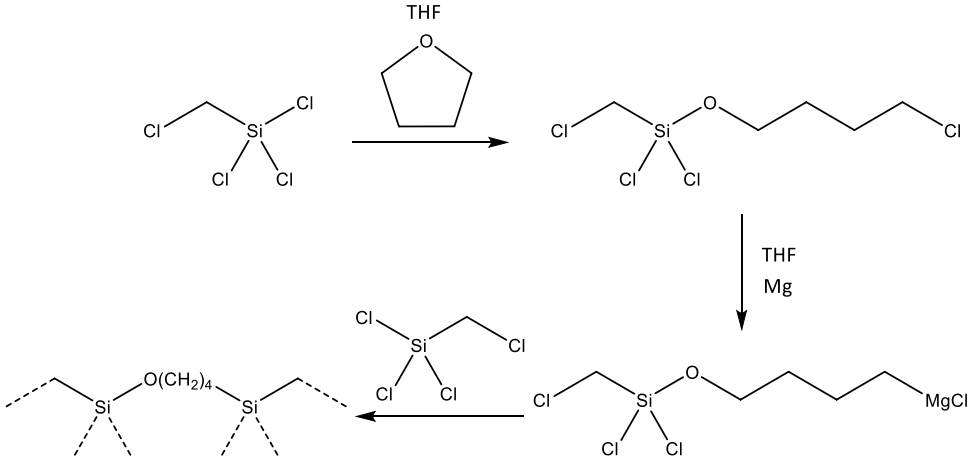

in Fig. 25. The second peak is mostly from water and some larger carbosilane fragments. The CO_2 and water are most likely contaminants condensed from the background atmosphere in the TVA line when the liquid nitrogen is placed on the sub-ambient trap.

3.4.3 Cold-Ring Fraction and Residue FTIR Analysis

Species that are volatilised at furnace temperatures but condense at temperatures below 5 °C were collected in the cold-ring fraction (CRF) with the water jacket. The cold-ring fraction and the residues were analysed after each heating event using FTIR-ATR spectroscopy. The IR bands were assigned and are reported in Table 4.

From 160 °C to 500 °C, species were collected in the cold-ring section and analysed using FTIR-ATR (Fig. 26). These fragments are oligomers or larger chain fragments that have too high a boiling point to be vaporised through the TVA line. There were no products collected in the cold-ring fraction at 650 °C. This is due to the material being an almost complete 3-D network of SiC with only smaller groups being cleaved which are volatile at CRF temperatures. At 160 °C the cold-ring fraction compares closely to the unreacted AHPCS material (Fig. 27), suggesting that low molecular mass oligomeric species are evaporated in this first heating step. The C = C stretching vibration at 1628 cm^{-1} is evident in the cold-ring fraction which shows it is from the unreacted form of the AHPCS. The residue at 160 °C (Figs. 27 and 28) shows a decrease in both the

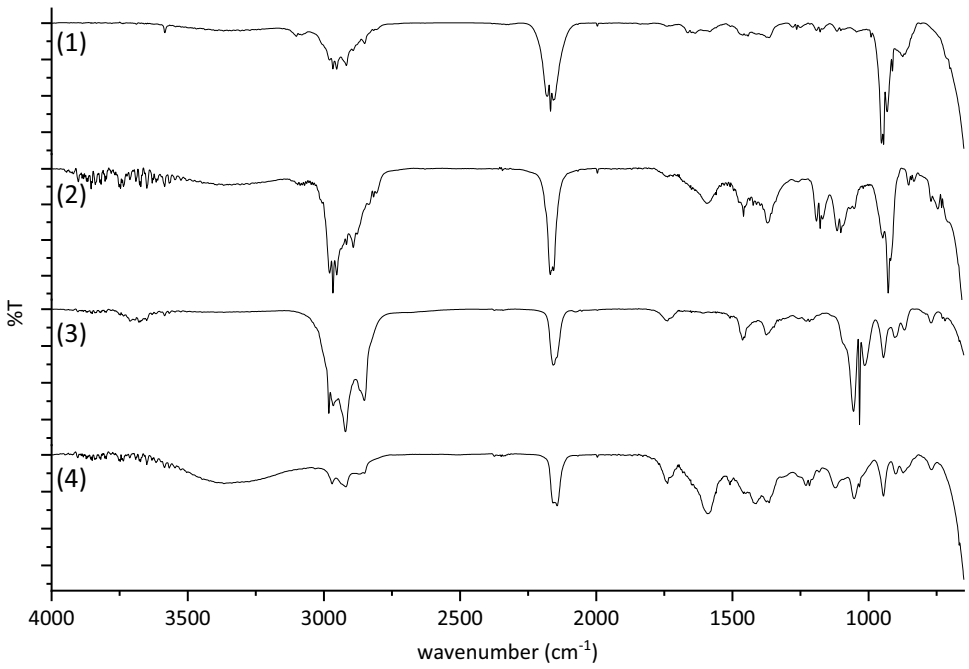

Fig. 19 FTIR gas phase spectra of the volatile SAD products in fractions 1, 2, 3 and 4 from the 300 °C isothermal TVA

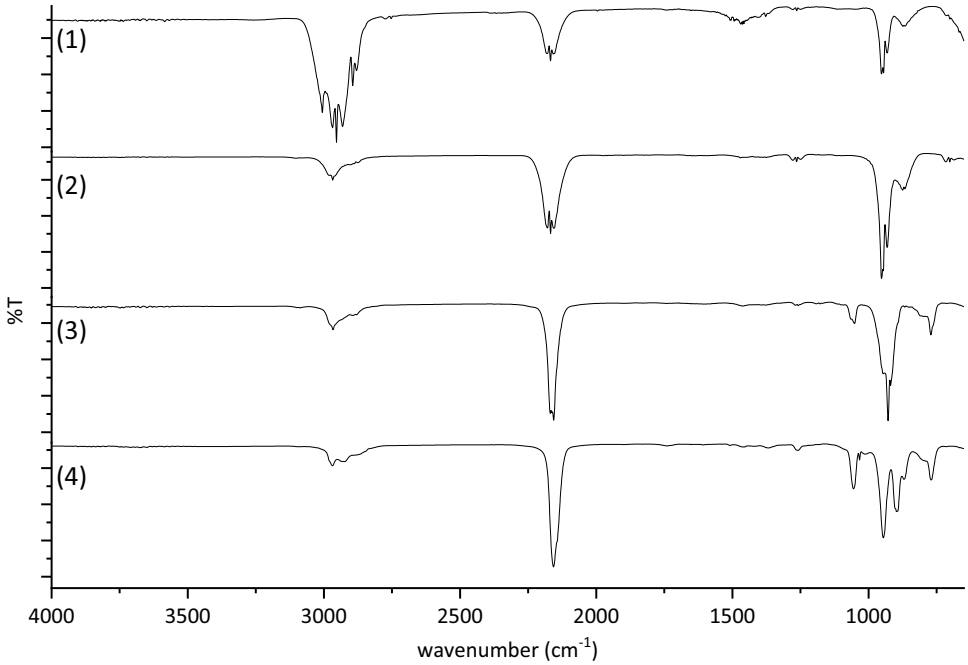

Fig. 20 FTIR gas phase spectra of the volatile SAD products in fractions 1, 2, 3 and 4 from the 500 °C isothermal TVA

1628 cm^{-1} and the vinylidene (-C = CH_2) stretching vibrations at 890 cm^{-1}. This is evidence of the cross-linking through the reaction of the allyl group. The silicon-to-hydrogen stretching vibration at 2113 cm^{-1} decreases marginally, consistent with the MS data for the non-condensable volatile products that shows the evolution of hydrogen. This suggests that the Si–H and C-H dehydrocoupling provides a pathway for the subsequent formation of new Si–C and Si–Si bonds as per Schemes 2 and 3. By 300 °C, the C = C peaks are lost completely indicating their complete incorporation into the network. The CRF from the isothermal heating at 300 °C is like that at 160 °C but seems to lack the C = C peak at 1628 cm^{-1}, suggesting that the oligomers in this case come from pyrolysis of the network rather than from low molecular mass AHPCS. This is consistent with the observation of chain fragments in the gaseous products. The 500 °C residue shows a large reduction in the aliphatic carbon-to-hydrogen stretching bands at ~ 2900 cm^{-1} and silicon-to-hydrogen stretching band at 2113 cm^{-1}. The disilylmethylene band at 1034 cm^{-1} shows an increase which is a result of the formation of silicon-to-carbon bonds by dehydrocoupling although the peak at 1250 cm^{-1} is evidence of the continuing

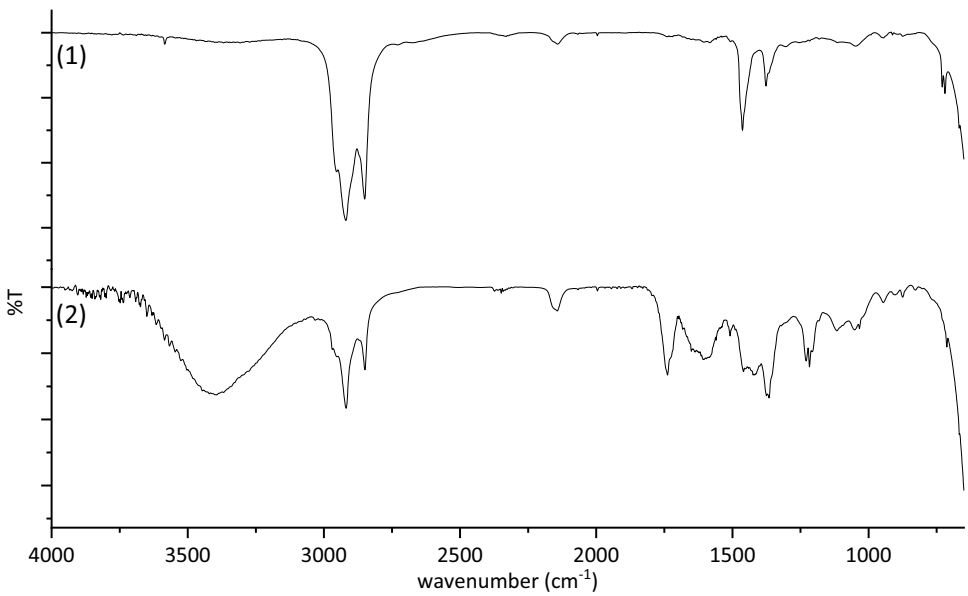

Fig. 21 FTIR gas phase spectra of the volatile SAD products in fractions 1 and 2 from the 650 °C isothermal TVA

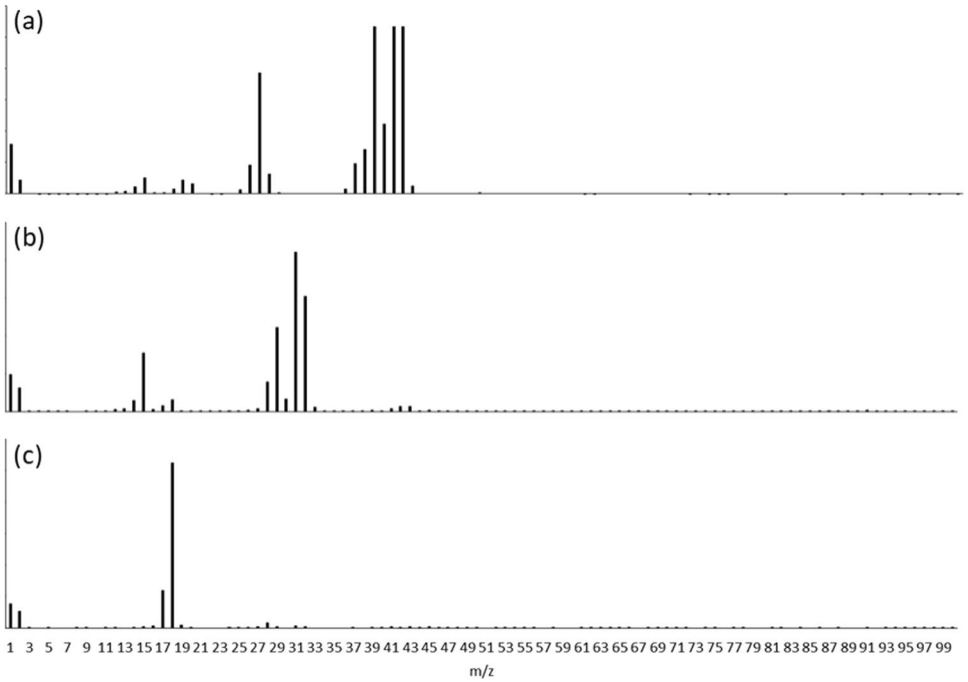

Fig. 22 MS of SAD products from 160 °C isothermal showing the presence of propene (**a** – fraction 1), methanol (**b** – fraction 2), and water (**c** – fraction 3)

presence of Si-CH_3 groups. The cold-ring fraction produced from the stepwise isothermal at 500 °C has an even larger aliphatic region in the IR spectrum compared to 300 °C, with an appearance of a peak at 1460 cm^{-1} corresponding

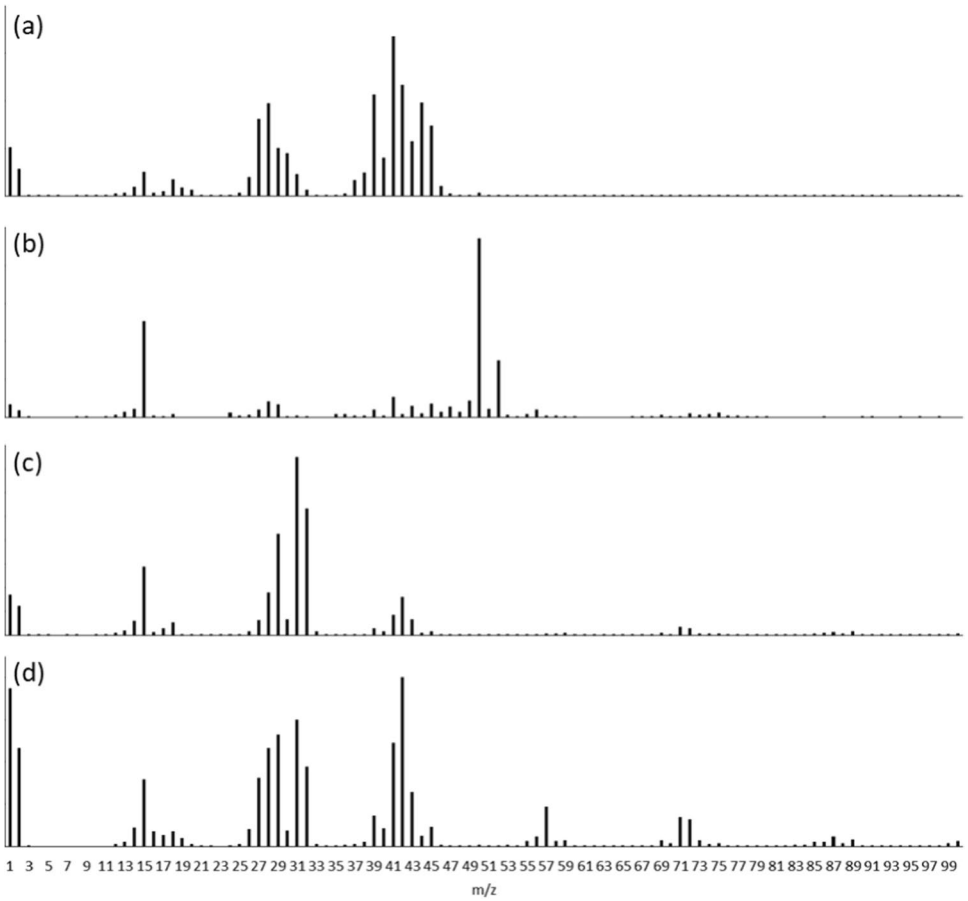

Fig. 23 MS of SAD products from 300 °C isothermal showing the presence of methyl silane and propene (**a** – fraction 1), chloromethane (**b** – fraction 2), methanol (**c** – fraction 3), and THF and large polycarbosilane fragments (**d** – fraction 4)

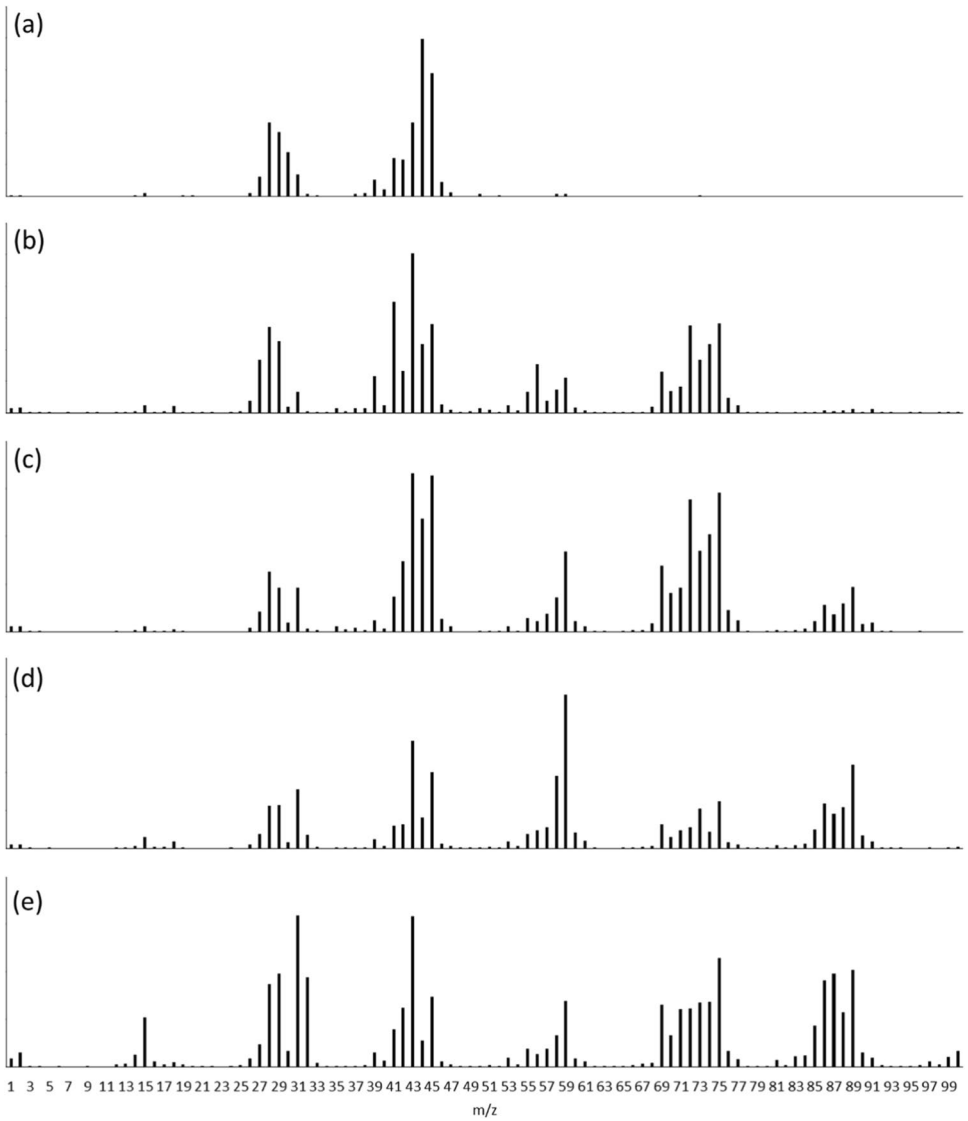

Fig. 24 MS of SAD products from 500 °C isothermal showing the presence of methyl silane (**a** – fraction 1), propene and ether alkyl silanes (**b** – fraction 2), propylsilane and silyl ethers (**c**, **d** – fraction 3), and large polycarbsosilane fragments (**e** – fraction 4)

to methyl end groups. This peak shows evidence of a larger proportion of aliphatic groups present in the lower molecular mass chain fragments as well as smaller fragments (more terminal groups). Significantly, the Si–H band is present in

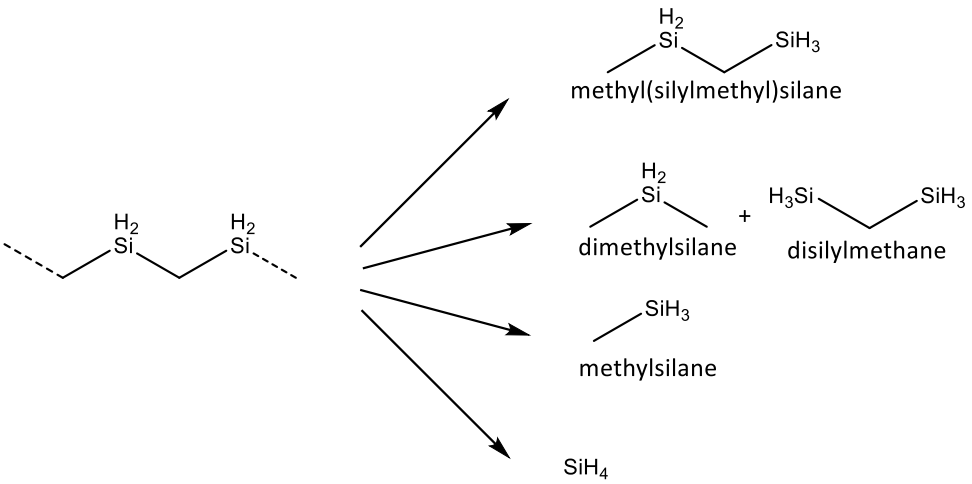

Scheme 5 Degradation products of the AHPCS main polymer backbone

Scheme 6 Degradation of bridging alkyl and hydrosilation cross-linked groups into propyl silane, propene and propane

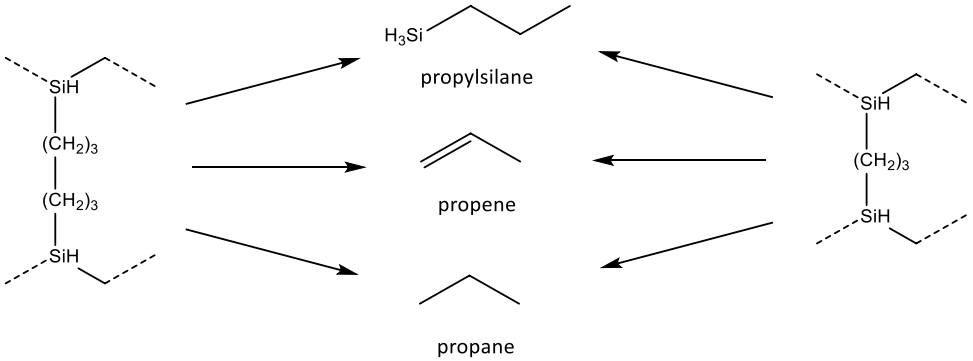

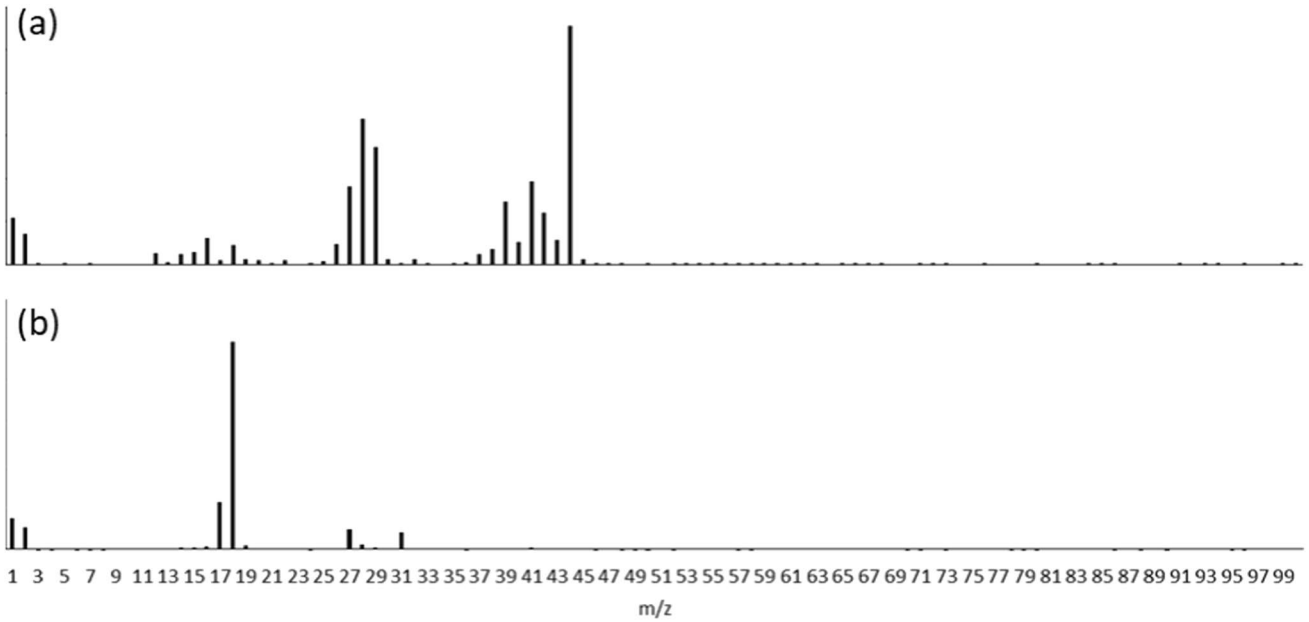

Fig. 25 MS of SAD products from 650 °C isothermal showing the presence of propene and propane (**a** – fraction 1), and background water (**b** – fraction 2)

the CRF indicating that not all the Si is retained in the residue. By 650 °C the spectrum changes completely with the absence of most of the characteristic peaks. The aliphatic bands at ~ 2900 cm^{-1} associated with C-H stretching are not present as well as the aliphatic bands between 1400 cm^{-1} and 1200 cm^{-1}. The Si-CH_2-Si bridges have disappeared at 1034 cm^{-1} owing to the cleavage of hydrogen and the formation of Si–C bonds. This is also inferred from the disappearance of the silicon-hydrogen stretching band. The only peak present is the one corresponding to the silicon-to-carbon stretching bands in SiC (825 cm^{-1}). This shows the complete formation of amorphous SiC by 650 °C. Throughout the FTIR spectra of the residues the baseline in the region from 1200 cm^{-1} to 650 cm^{-1} shifts higher and this is partly due to the change in refractive index of the material as it cross-links and forms SiC. The refractive index of the sample must be lower than the diamond ATR crystal otherwise light is lost to the sample. The colour darkens until it forms the black

Table 4 FTIR band assignments for AHPCS CRF and residue [14, 30, 31]

Wavenumber (cm^{-1})	Assignment
3075, 2994	C = CH_2 (C-H) stretching
2968, 2951, 2918, 2911, 2875, 2850, 2832	CH_2, CH_3, CH stretching
2113	Si–H stretching
1628, 1188, 1156	Si-CH_2-CH = CH_2 (C = C) stretching
1457	CH_3 bending
1417,1390	Si-CH_2-CH = CH_2 (CH_2) bending
1406	Si-$(CH)_6$-Si (C-H) bending
1354	Si-CH_2-Si deformation
1251	Si-CH_3 deformation
1156, 1188	Si-CH_2-CH = CH_2 deformation
1140	Si-$(CH)_6$-Si deformation
1034	Si-CH_2-Si stretching
945, 929	Si–H bending
890	C = C bending
825, 745	Si–C stretching

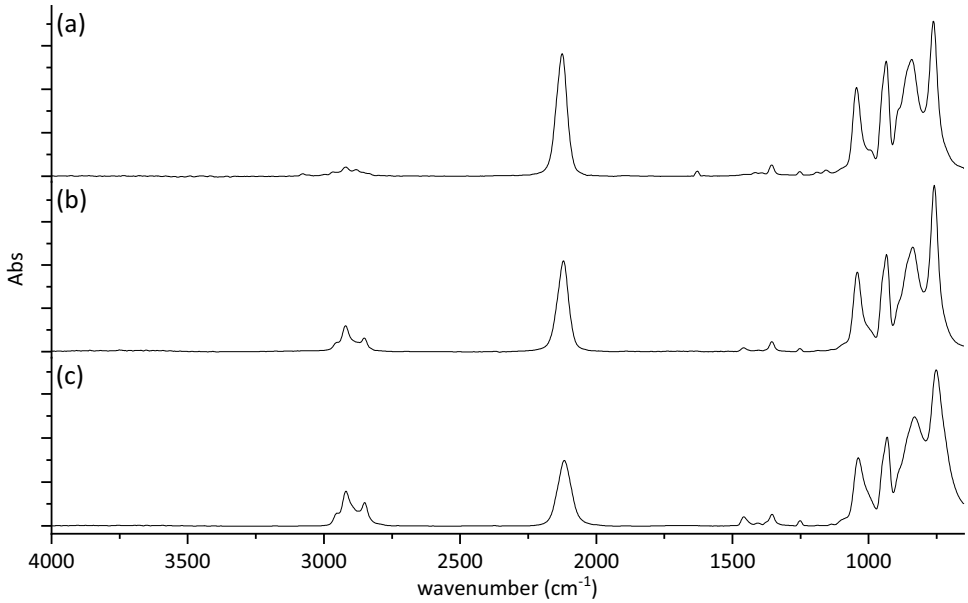

Fig. 26 FTIR-ATR spectra of CRFs formed upon the isothermal TVAs at 160 °C (**a**), 300 °C (**b**) and 500 °C (**c**)

SiC which has an increased refractive index of 2.64, which is higher than diamond at 2.42 [32, 33].

3.4.4 SSNMR Residue Analysis

^{13}C and ^{29}Si SSNMR was conducted on the residue from each isothermal heating step and the data are shown in Fig. 29 and 30.

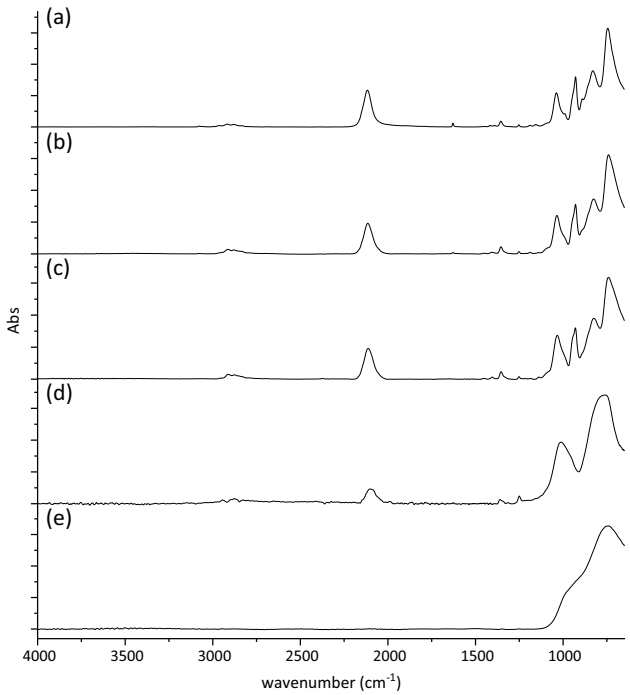

Fig. 27 FTIR-ATR spectra of AHPCS (**a**) and residues formed upon the isothermal TVAs at 160 °C (**b**), 300 °C (**c**), 500 °C (**d**) and 650 °C (**e**)

The ^{13}C spectrum from the residue generated at 160 °C shows narrow peaks present 134, 115 and 51 ppm. The 134 and 115 ppm peaks correspond to the =CH and $=CH_2$ on the allyl group, respectively. The peak at 51 ppm represents the methylene group adjacent to the C=C. These narrow peaks represent greater molecular mobility of the groups present on the polymer chain which is lessened as the polymer changes to forms the SiC network. These peak positions and changes correspond to be consistent with previous findings [30]. The peak groupings around 20 and 0 ppm that dominate the spectra are consistent with Si-CH_2-Si and H_3C-Si groups. There are some changes observed in the ^{13}C spectra between the residues generated at 160 and 300 °C, most notably the absence of the C=C signals as a result from the cross-linking of allyl groups. There is a slight increase in the methylene group signal consequently. There is also an increase of the C-Si group at 20 ppm. This may be from the minor Si–C recombination occurring at 300 °C. Between the 300 and 500 °C spectra there are major changes, with only the Si–C and C-H groups being observed. The groups at the lower ppm range (-14 to -5 ppm), which correspond to -CH_2/CH_3 groups, have disappeared with the presence of a larger broader peak observed at 3 ppm representing $HCSi_3$ moieties. The peak broadening is typical of a rigid, disordered material, which correlates to the amorphous SiC network. This coincides with the cleavage of C-H bonds producing higher substituted carbons in the network. The smaller group at 17 ppm is most likely from CSi_4 moieties which have formed from the full recombination of carbon. The larger group at 0 ppm is more representative of C-H species still present throughout the material, as evident from the FTIR in Fig. 27. At 650 °C the material spectrum consists of only one broad featureless peak at 17 ppm. This fully corresponds

to the CSi_4 species, which shows that all the carbon and silicon atoms have recombined to form the amorphous SiC.

The ^{29}Si spectrum at 160 °C shows three major groupings of peaks, with the narrow bands again representing greater molecular mobility in the polymer. The assignments of the groups are based on assignments in previous work. Two of the groups of signals are split into multiplets. The region around -60 ppm consists of two quartets, which is consistent with the trihydridosilicon ($CSiH_3$) species. The region around -40 ppm consists of triplets, which are also consistent with dihydrodidosilicon (C_2SiH_2) species. The smallest grouping of peaks is associated with the monohydridosilicon (C_3SiH) species around -15 ppm [29]. The 300 °C spectrum shows very few changes in comparison to the 160 °C spectrum, with a slight increase in the SiH region in comparison to the SiH_2 and SiH_3. This is consistent with the loss of hydrogen observed from the TVA, with only small volumes produced from the cleavage of hydrogen from SiH_2 and SiH_3 species. The most significant change occurs between the 300 and 500 °C spectra. The peaks corresponding to SiH_3 have almost completely disappeared and the -SiH_2 species have shown a sizeable decrease and shift. This will be because of recombination of higher hydrogenated silicon groups, SiH_3, forming SiH_2 species which then again subsequently cleave a hydrogen atom to form SiH species. This dehydrocoupling may result in this shift and produce Si–Si recombination as well as Si–C which is consistent with previous work [15]. Yu et al. note that the reactivity of the Si–H bond to hydrosilation and dehydrocoupling reactions decreases in the order $SiH_3 > SiH_2 > > SiH$, consistent with our observations [16]. A new peak is observed at 1 ppm which is consistent with the formation of SiC_4 [34, 35]. The broadness of the peak indicates a rigid disordered material, which is consistent with the formation of amorphous SiC. The last spectrum shows only a single peak observed at -2 ppm. This shows the final conversion of the SiH species in to SiC_4 [36, 37].

3.5 XRD Analysis of AHPCS

The range picked was used to compare the crystallisation of the SiC with increasing temperature, which is shown in Fig. 31. The temperatures were selected for observing the formation of the initial crystalline β-SiC (1100 °C) and its subsequent increase in crystallinity from heating until the conversion to α-SiC (1700° C).

The XRD pattern observed at 1100 °C shows peaks which are concurrent with the major peaks of SiC (36°, 60°, 72°) [38]. These peaks occur in both β- and α-SiC but it is most likely from to the β polytype due to the absence of other peaks and lower crystallisation temperature. As has been reported in the literature the crystallisation of the

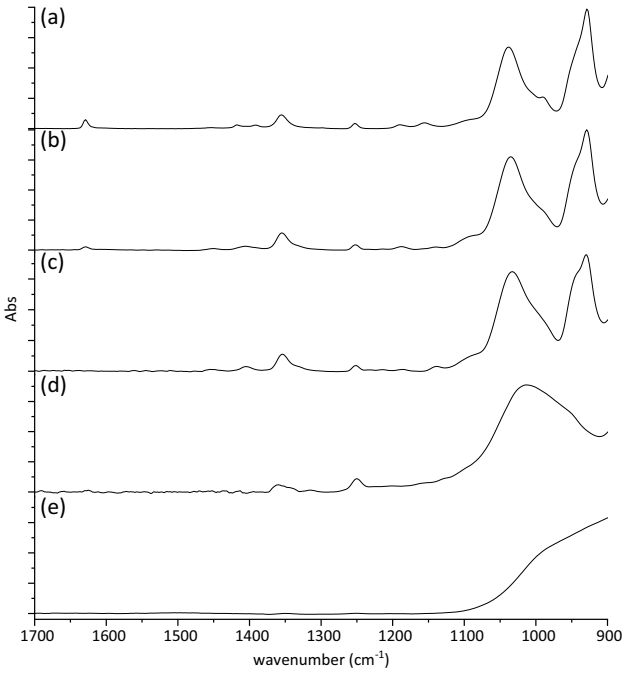

Fig. 28 FTIR-ATR spectra of AHPCS (**a**) and residues formed upon the isothermal TVAs at (**a**), 160 °C (**b**), 300 °C (**c**), 500 °C (**d**) and 650 °C (**e**) zoomed to 1700—900 $cm.^{-1}$

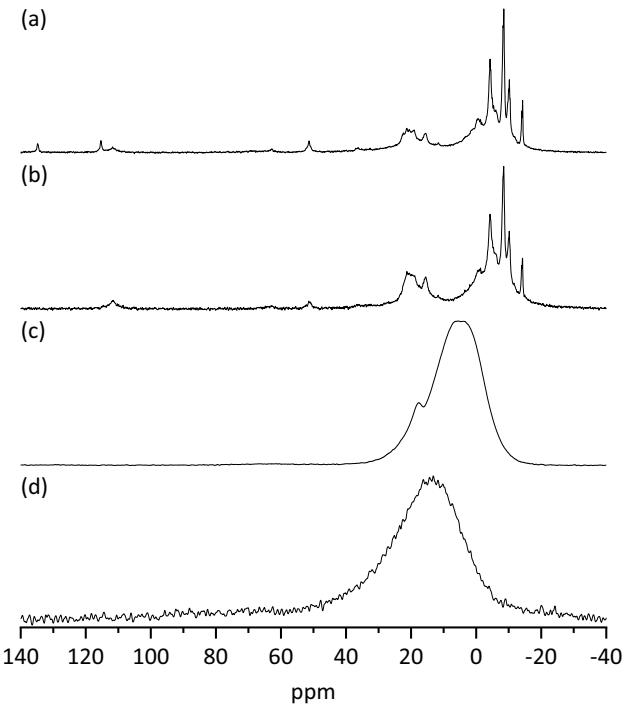

Fig. 29 Solid-state.^{13}C NMR spectra of residues generated upon heating to (**a**) 160 °C, (**b**) 300 °C (**c**) 500 °C and (**d**) 650 °C (The group at 111 ppm is due to the PTFE rotor caps present in the NMR instrument)

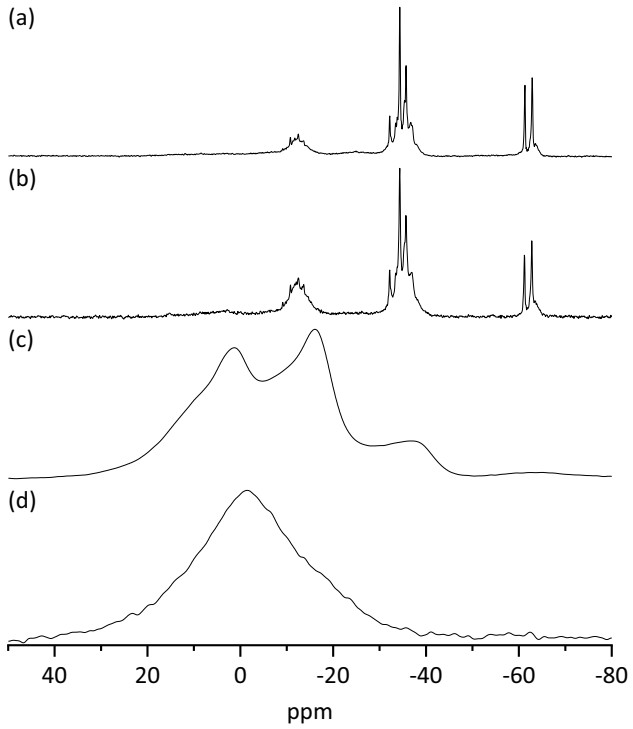

Fig. 30 Solid-state ^{29}Si NMR spectra of residues generated upon heating to (**a**) 160 °C, (**b**) 300 °C (**c**) 500 °C and (**d**) 650 °C

amorphous SiC increases with temperature, evident with the main peaks in XRD pattern [14, 39, 40]. As the temperature is increased to 1500 °C, differentiation appears in the XRD pattern. Peaks at ~ 41° and ~ 75° appear which correspond to the α polytype, and the peaks at 60° and 72° show a slight shift to a higher diffraction angle which occurs from the rearrangement of β to from the α-SiC. There is no evidence of oxidation occurring in the sample, with no major SiO_2 peaks being present (22° for SiO_2) [41]. Due to the particle size of the sample, the peaks have a low resolution, but the major peaks can still be identified.

The crystallisation of SiC is shown to occur at temperatures above 1100 °C and increases with temperature, the β polytype is formed at lower temperatures and the rearrangement occurs at temperatures between 1300 and 1500 °C. At temperatures higher than 1500 °C, the α polytype becomes the dominant polytype due to it being the thermodynamically favourable state.

The complete predicted reaction intermediates are shown in Scheme 7 with a generalised structure for each thermal process and finished crystalline structure.

4 Conclusion

Thermal volatilisation analysis was carried out on AHPCS to determine the reaction processes occurring during ceramicisation of a pre-ceramic polymer. Four different isothermal TVA analyses were carried out, each corresponding to a significant step in the ceramicisation process. Cross-linking is initiated at 160 °C through the allyl groups by radical reactions, by dehydrocoupling and by hydrosilation

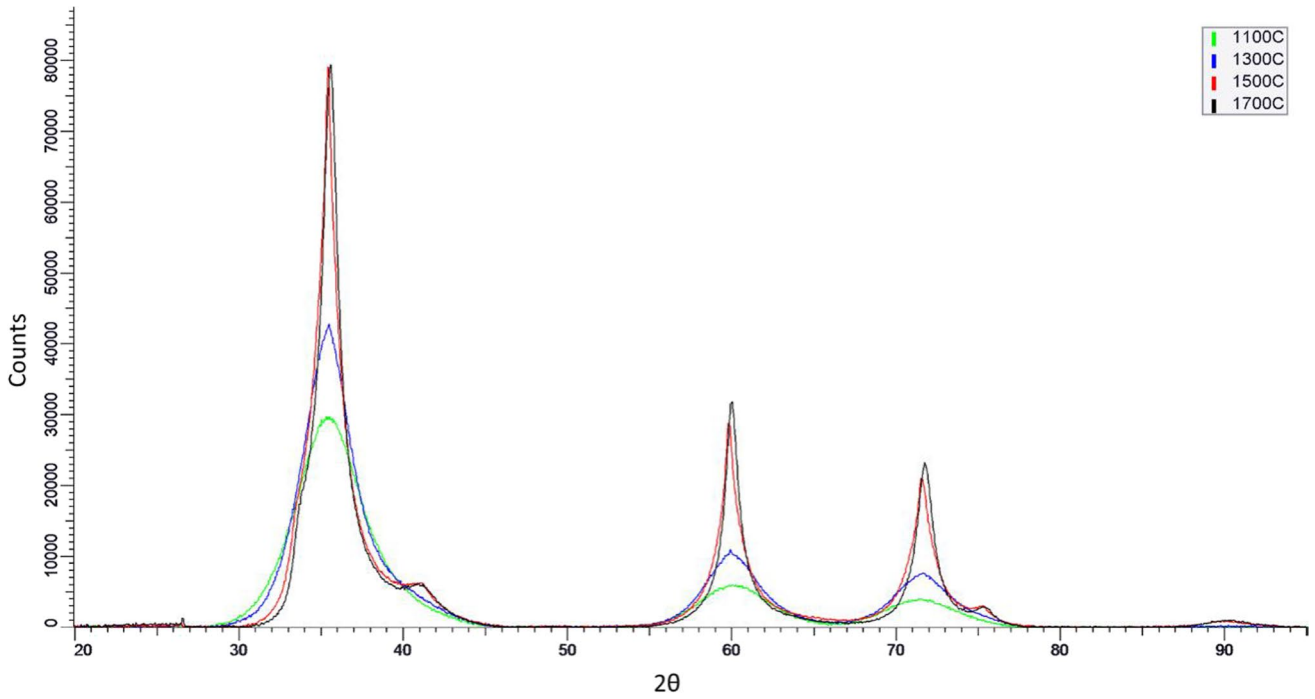

Fig. 31 XRD Pattern of AHPCS heated at 1100 °C (green), 1300 °C (blue), 1500 °C (red), 1700 °C (black)

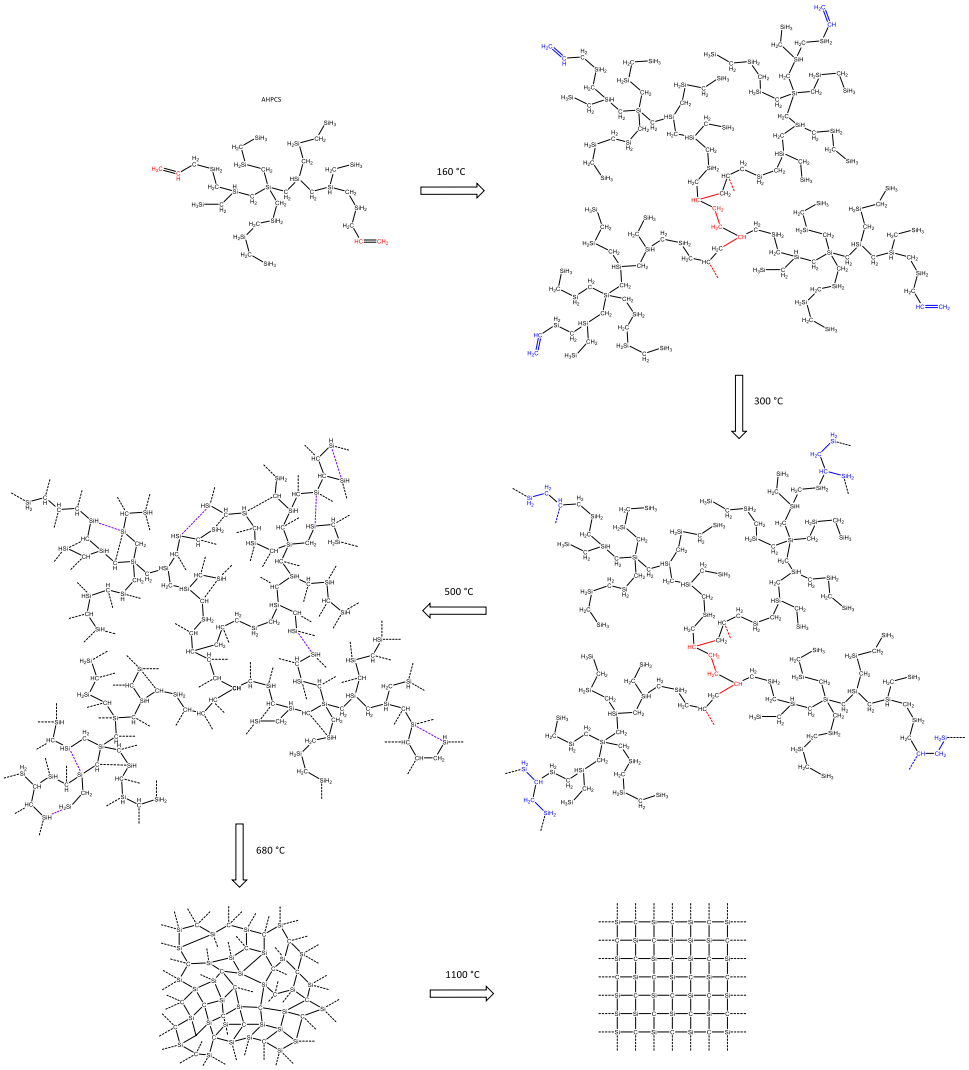

Scheme 7 Complete predicted thermal event reaction intermediates to form crystallised SiC from AHPCS. Red representing the initial cross-linking, blue representing the hydrosilation of the allyl groups, and purple representing the Si–Si dehydrocoupling recombination reactions

that produce a lightly cross-linked polymer with additional cross-linking believed to occur through combination of Si radicals produced by homolytic scission of Si–H bonds. Some of the other volatiles are believed to be a result of the synthesis, such as propene being present due to residual uncross-linked material. Methanol and water are also present due to side reactions with the THF solvent during synthesis. Low molecular mass oligomers also seen volatilise from the AHPCS. The allyl groups completely react or are removed from the polymer by 300 °C with the complete disappearance of the double bonds. Small side groups are released through scission and cleavage producing hydrogen, methane and ethane. Alkyl silanes are volatilised as a result of weakly bonded chain end groups in the main polymer network. This shows evidence of light chain scission with a higher proportion of aliphatic groups seen in the CRF. More methanol is observed which may be from cleavage of silylether groups, as well as chloromethane from the Grignard synthesis—most likely from Si-Cl terminal groups left unreacted in the structure. The ceramicisation process occurs at temperatures above 300 °C, with further formation of new Si–C bonds as a result of combination of radicals produced by homolytic scission of Si–H and C-H or C–C bonds.

The volatiles released during this process change from mostly hydrogen at 160 °C, from dehydrocoupling, to methane/methanol/SiH_4 by 350 °C, from C–C and C-O cleavage. Hydrogen once again becomes the major volatile product above 400 °C due to higher proportion of dehydrocoupling forming Si–C and Si–Si bonds. Small chain fragments are seen in the form of larger alkyl silanes. These fragments come from the chain scission of the polymer at weaker parts of the network. The process of side group scission leads to further radical recombination reactions of silicon and carbon atoms to build the SiC network. By 650 °C the polymer has completed its rearrangement into amorphous SiC. The volatiles released are mostly hydrogen with very few condensable products seen. SiC is then crystallised at higher temperatures forming β-SiC

at 1100 °C and then subsequently α-SiC above 1500 °C. These results show the distinct processes occurring with specifics to which groupings recombine first in the ceramicisation. This may be used to develop better pre-ceramic materials by decreasing the volatiles produced and making a more efficient ceramic precursor.

Acknowledgements LJP thanks Sandvik Ltd T/A Kanthal for the award of a PhD studentship.

Authors' Contributions The work reported in this manuscript forms part of the PhD research of the first author, Lewis Print, supervised by John Liggat. Authors LJP, JJL, SM and HS contributed to the study conception and design. Material preparation, data collection and analysis were performed by LJP except for the solid-state NMR data collected by DCA. The first draft of the manuscript was written by LJP and it was commented on by JJL. All authors read and approved the final manuscript.

Funding This work was supported Sandvik Ltd T/A Kanthal and the Strathclyde Centre for Doctoral Training in Advanced Functional and Engineering Polymers.

Data Availability The data required to reproduce these findings are available to download from PURE at the University of Strathclyde (https://doi.org/10.15129/5bef7bd0-535e-4590-9eb9-3112e6493001).

Declarations

Ethics approval Not applicable.

Consent to participate Not applicable.

Consent for publication Consent for publication has been given by Sandvik Ltd T/A Kanthal.

Competing interests The authors have no relevant financial or non-financial interests to disclose.

Research involving Human Participants and/or Animals Not applicable.

Informed Consent Not applicable.

Disclosure of potential conflicts of interest The authors have no relevant conflicts of interests to disclose.

References

1. Choyke W, Matsunami H, Pensl G (2004) Silicon Carbide Recent Major Advances, 1st edn. Springer-Verlag, New York NY
2. Oliveros A, Guiseppi-Elie A, Saddow S (2013) Silicon carbide: a versatile material for biosensor applications. Biomed Microdevices 15:353–368. https://doi.org/10.1007/s10544-013-9742-3
3. Kimoto T, Cooper JA (2014) Applications of Silicon Carbide Devices in Power Systems. Fundamentals of Silicon Carbide Technology, 1st edn. John Wiley & Sons, Singapore, pp 445–486
4. Yoon T-H, Hong L-Y, Kim D-P (2011) Preparation and Applications of Ceramic Composite Phases from Inorganic Polymers. In: Woo H-G, Li H (eds) Advanced Functional Materials. Springer, Berlin/Heidelberg, pp 103–156
5. Choyke W, Pensl G (1997) Physical Properties of SiC. MRS Bull 22:25–29. https://doi.org/10.1557/S0883769400032723
6. Acheson E (1893) Production of artificial crystalline carbonaceous materials, US Patent 492767, 28th February 1893
7. Acheson E (1893) Carborundum: Its history, manufacture and uses. J Franklin Inst 136:194–203
8. Riedel R, Passing G, Schönfelder H (1992) Synthesis of dense silicon-based ceramics at low temperatures. Nature 355:714–717. https://doi.org/10.1038/355714a0
9. Schilling CL, Wesson JP, Williams TC (1983) Polycarbosilane precursors for silicon carbide. J Polym Sci Polym Symp 70:121–128. https://doi.org/10.1002/polc.5070700110
10. Birot M, Pillot JP, Dunoguès J (1995) Comprehensive Chemistry of Polycarbosilanes, Polysilazanes, and Polycarbosilazanes as Precursors of Ceramics. Chem Rev 95:1443–1477. https://doi.org/10.1021/cr00037a014
11. Bouillon E, Langlais F, Pailler R, Naslain R, Cruege F, Huong PV, Sarthou JC, Delpuech A, Laffon C, Lagarde P et al (1991) Conversion mechanisms of a polycarbosilane precursor into an SiC-based ceramic material. J Mater Sci 26:1333–1345. https://doi.org/10.1007/BF00544474
12. Li H, Zhang L, Cheng L, Wang Y, Yu Z (2008) Polymer–ceramic conversion of a highly branched liquid polycarbosilane for SiC-based ceramics. J Mater Sci 43:2806–2811. https://doi.org/10.1007/s10853-008-2539-8
13. Li H, Zhang L, Cheng L, Wang Y, Yu Z, Huang M, Tu H, Xia H (2008) Effect of the polycarbosilane structure on its final ceramic yield. J Eur Ceram Soc 28:887–891. https://doi.org/10.1016/j.jeurceramsoc.2007.07.020
14. Sreeja R, Swaminathan B, Painuly A, Sebastian T, Packirisamy S (2010) Allylhydridopolycarbosilane (AHPCS) as matrix resin for C/SiC ceramic matrix composites. Mater Sci Eng 168:204–207. https://doi.org/10.1016/j.mseb.2009.12.033
15. Kaur S, Riedel R, Ionescu E (2014) Pressureless fabrication of dense monolithic SiC ceramics from a polycarbosilane. J Eur Ceram Soc 34:3571–3578. https://doi.org/10.1016/j.jeurceramsoc.2014.05.002
16. Yu Z, Min H, Zhan J, Yang L (2012) Preparation and dielectric properties of polymer-derived SiCTi ceramics. Ceram Int 39:3999–4007. https://doi.org/10.1016/j.ceramint.2012.10.250
17. Li M, Yoon TH, Kim DP (2010) Novel Inorganic Polymer Derived Microfluidic Devices: Materials, Fabrication, Microchemical Performance. Proc 7th Int Conf Nanochannels, Microchannels, Minichannels 2009, ICNMM2009 1279–1286. https://doi.org/10.1115/ICNMM2009-82136
18. Nader M, Aldinger F, Hoffmann MJ (1999) Influence of the α/β-SiC phase transformation on microstructural development and mechanical properties of liquid phase sintered silicon carbide. J Mater Sci 34:1197–1204

19. McNeill IC (1966) Thermal volatilization analysis: A new method for the characterization of polymers and the study of polymer degradation. J Polym Sci Part A-1 Polym Chem 4:2479–2485. https://doi.org/10.1002/pol.1966.150041012
20. Interrante LV, Whitmarsh CW, Sherwood W, Wu H-J, Lewis R, Maciel G (1994) High yield polycarbosilane precursors to stoichiometric SiC. Synthesis, pyrolysis and application. MRS Online Proc Libr 346:593–603
21. Sorarù GD, Suttor D (1999) High temperature stability of sol-gel-derived SiOC glasses. J Sol-Gel Sci Technol 14:69–74. https://doi.org/10.1023/A:1008775830830
22. Hurwitz F (1998) 22nd Annual Conference on Composites, Advanced Ceramics, Materials, and Structures: B: Ceramic Engineering and Science Proceedings, Volume 19, Issue 4. In: Bray D (ed) Filler/polycarbosilane systems as CMC matrix percursors. John Wiley & Sons Inc, Hoboken, NJ, USA, pp 267–274
23. Interrante L, Moraes K (2002) Mechanical, thermochemical, and microstructural characterization of AHPCS-derived SiC. In: Kohyama A, Singh M, Lin H-T, Katoh Y (eds) SiC/SiC ceramic composites: developments and applications in energy systems, ceramic transactions. Wiley, NY, pp 125–140
24. Nguyen CT, Hong L-Y, Kim D-P, Lee J-Y, Woo H-G (2006) Facile Synthetic Route of Polycarbosilane as a SiC Precursor with Zeolite Catalysts. J Ceram Soc Japan 114:487–491. https://doi.org/10.2109/jcersj.114.487
25. Nair SG, Subramania Siva M, Thomas D, Sreejith KJ, Prabhakaran PV, Devasia R (2019) Liquid polycarbosilane as a potential chemical liquid vapour deposition precursor for SiC. Ceram Int 45:17442–17446. https://doi.org/10.1016/j.ceramint.2019.05.305
26. Shukla SK, Tiwari RK, Ranjan A, Saxena AK, Mathur GN (2004) Some thermal studies of polysilanes and polycarbosilanes. Thermochim Acta 424:209–217. https://doi.org/10.1016/j.tca.2004.06.003
27. Huber M, Harvey A (2016) Thermal conductivity of gases. In: Haynes W (ed) CRC handbook of chemistry and physics, 97th edn. CRC Press, Boca Raton FL, p 1305
28. Shen Q (2010) Composition, preparation of polycarbosilanes and their uses, US Patent 7714092B2, 11th May 2010
29. Huang M, Fang Y, Li R, Huang T, Yu Z, Xia H (2009) Synthesis and properties of liquid polycarbosilanes with hyperbranched structures. J Appl Polym Sci 113:1611–1618. https://doi.org/10.1002/app.30071
30. Interrante LV, Whitmarsh CW, Sherwood W, Wu H-J, Lewis R, Maciel G (1995) Hydridopolycarbosilane Precursors to Silicon Carbide. Applications of Organometallic Chemistry in the Preparation and Processing of Advanced Materials. Springer, Netherlands, Dordrecht, pp 173–183
31. Launer PJ, Arkles B (2013) Infrared analysis of organosilicon compounds: spectra-structure correlations. In: Arkles B, Larson GL (eds) Silicon compounds: silanes & silicones, 3rd edn. Gelest Inc, Morrisville, PA, pp 175–178
32. Singh S, Potopowicz JR, Van ULG, Wemple SH (1971) Nonlinear optical properties of hexagonal silicon carbide. Appl Phys Lett 19:53. https://doi.org/10.1063/1.1653819
33. Phillip HR, Taft EA (1964) Kramers-Kronig Analysis of Reflectance Data for Diamond. Phys Rev 136:. https://doi.org/10.1103/PhysRev.136.A1445
34. Soraru GD, Babonneau F, Mackenzie JD (1990) Structural evolutions from polycarbosilane to SiC ceramic. J Mater Sci 25:3886–3893. https://doi.org/10.1007/BF00582455
35. Ly HQ, Taylor R, Day RJ, Heatley F (2001) Conversion of polycarbosilane (PCS) to SiC-based ceramic: Part 1. Characterisation of PCS and curing products. J Mater Sci 36:4037–4043. https://doi.org/10.1023/A:1017942826657
36. Blinka TA, Helmer BJ, West R (1984) Polarization Transfer NMR Spectroscopy for Silicon-29: The INEPT and DEPT Techniques. Adv Organomet Chem 23:193–218. https://doi.org/10.1016/S0065-3055(08)60611-5
37. Uhlig F, Marsmann HC (2008) Si NMR some practical aspects. In: Gelest Catalog, Gelest Inc, Morrisville, PA, pp 208–222
38. Mas'udah K, Diantoro M, (2018) Synthesis and Structural Analysis of Silicon Carbide from Silica Rice Husk and Activated Carbon Using Solid-State Reaction. J Phys Conf Ser 1093:12033. https://doi.org/10.1088/1742-6596/1093/1/012033
39. Shih C, Tulenko JS, Baney RH (2011) Low-temperature synthesis of silicon carbide inert matrix fuel through a polymer precursor route. J Nucl Mater 409:199–206. https://doi.org/10.1016/j.jnucmat.2010.12.027
40. Mehr M, Moore DT, Esquivel-Elizondo JR, Nino JC (2015) Mechanical and thermal properties of low temperature sintered silicon carbide using a preceramic polymer as binder. J Mater Sci 50:7000–7009. https://doi.org/10.1007/S10853-015-9252-1
41. Joni IM, Nulhakim L, Vanitha M (2018) Characteristics of crystalline silica (SiO2) particles prepared by simple solution method using sodium silicate (Na2SiO3) precursor. J Phys Conf Ser 1080:12006. https://doi.org/10.1088/1742-6596/1080/1/012006